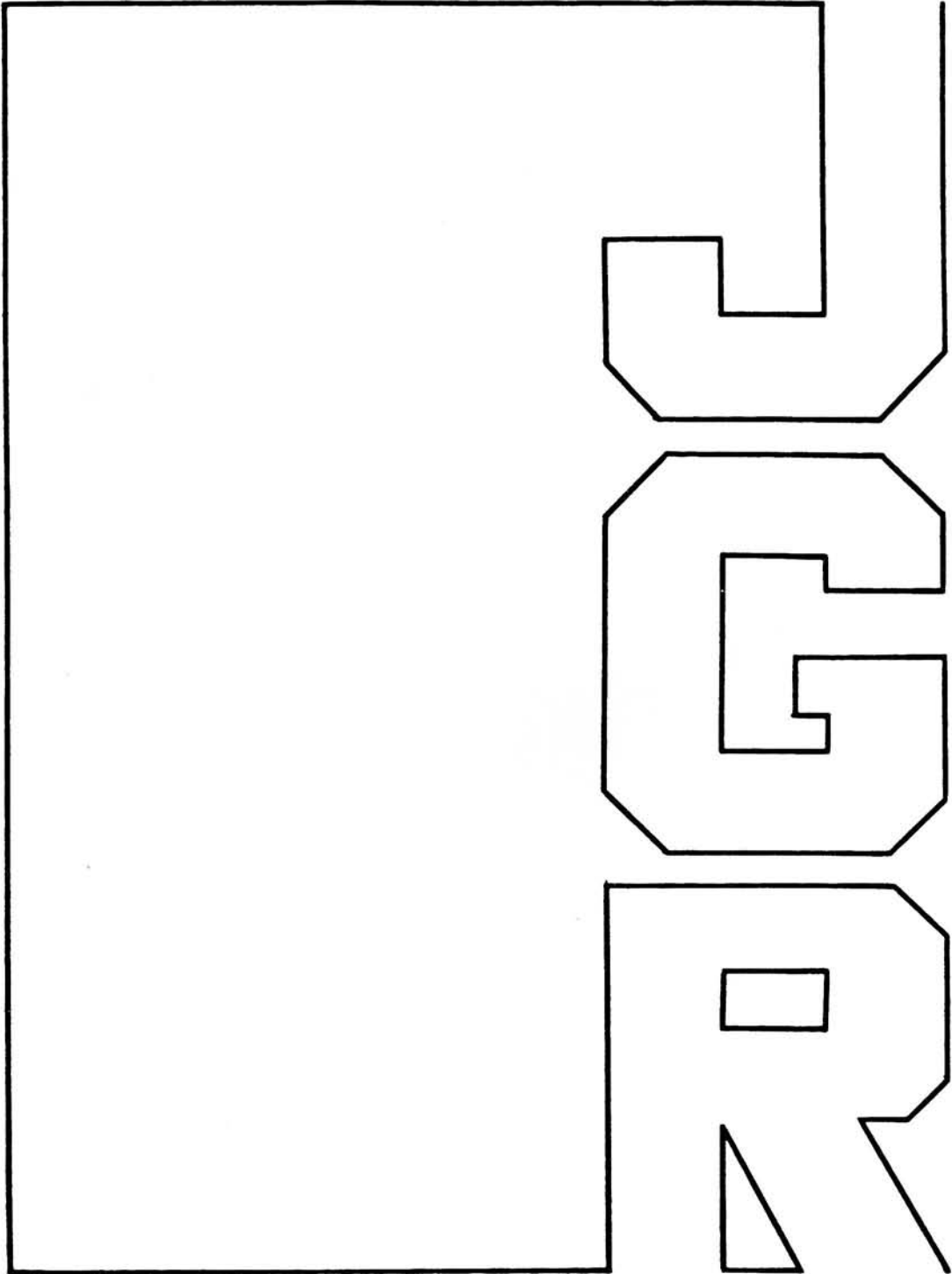


Ice-3G: A New Global Model Of Late Pleistocene Deglaciation Based Upon Geophysical Predictions Of Post-Glacial Relative Sea Level Change

A. M. TUSHINGHAM AND W.R. PELTIER



Ice-3G: A New Global Model Of Late Pleistocene Deglaciation Based Upon Geophysical Predictions Of Post-Glacial Relative Sea Level Change

A. M. TUSHINGHAM AND W.R. PELTIER

A new high resolution global model of late Pleistocene deglaciation is inferred on the basis of geophysical predictions of postglacial relative sea level variations in which the ice-ocean-solid Earth interaction is treated in a gravitationally self-consistent fashion. For the purpose of these analyses the radial viscoelastic structure of the planet is assumed known on the basis of previously published sensitivity tests on solutions of the forward problem. Only radiocarbon controlled relative sea level histories from sites that were actually ice covered (with one or two additions) are employed to constrain the model, leaving relative sea level (RSL) data from sites that were not ice covered to be employed to confirm its consistency. Results for these confirmatory analyses are reported elsewhere. Here the new deglaciation model, referred to as ICE-3G, is compared to previous models derived by several independent means and tested against a number of additional observations other than sea level histories, including geologically controlled retreat isochrones, oxygen-isotope data from deep-sea sedimentary cores, and coral terrace elevations. The latter two observations strongly constrain the net sea level rise that has occurred since the onset of deglaciation and therefore the mass of ice that melted during the last glacial-interglacial transition.

INTRODUCTION

Throughout Earth history the surface climate of the planet has varied dramatically. The precision with which we understand these past changes of climate is of course a strongly decreasing function of the age of the epoch within which the changes occurred. Generally speaking, the dominant cause of any given climate change within the Earth system is closely related to the governing time scale. Of all such variability the slowest of consequence is that driven by continental drift and thus ultimately related to the mantle convection process. On the shortest time scales, most climate variability can be traced to changes of composition and dynamics of the atmosphere-ocean subsystem. On "intermediate" timescales of thousands to hundreds of thousands of years we see clear evidence of extreme variations of surface climate that are ultimately caused by influences originating from outside the Earth system itself. Within the Pleistocene epoch, for example, which comprises roughly the past 2.4 million years of Earth history, the evidence is unequivocal that planetary climate is very significantly forced by small changes in effective solar insolation due to the variation with time of the geometry of the Earth's orbit around the Sun. On the basis of $\delta^{18}\text{O}$ measurements on foraminiferal tests from deep sea sedimentary cores, it is now quite clear that the volume of continental ice during this period has changed in sympathy with this orbital forcing [Shackleton, 1967; Hays *et al.*, 1976]. The notion that ice ages could be a consequence of this cause was of course originally due to Milankovitch [1941]. Although at least one serious problem exists with the conventional Milankovitch hypothesis [Hyde and Peltier, 1985, 1987], it is nevertheless now quite widely accepted. Our purpose in the present paper will be to exploit ideas from solid Earth geophysics in an effort to constrain the details of the last glacial-interglacial transition of the present ice age and hopefully to thereby provide an important physical constraint on models of Pleistocene climatic change.

The most important variable feature of Earth system climate throughout the Pleistocene epoch has been the extent to which the northern hemisphere continents near the rotation pole have been ice covered. Throughout the past 10^6 years, sea core $\delta^{18}\text{O}$ data demonstrate that successive glaciation-deglaciation cycles have occurred with monotonous 10^5 -year regularity. The last glacial maximum occurred 18,000 radiocarbon years before present (B.P.) and by 7000 ^{14}C years ago both the vast Laurentide ice sheet that covered all of Canada, and the northwestern European complex centred on the Gulf of Bothnia, which also covered both the Barents and Kara seas, had completely disappeared. In attempting to understand the details of the paleoclimatic change involved in the disintegration of these extensive complexes of land ice, it is clearly important to have as accurate a reconstruction as possible of where the dominant ice masses were initially and of how they retreated in time. The main goal of the present paper is to employ geophysical methods to infer a new global chronology of this late Pleistocene deglaciation event.

The main constraint that we shall invoke to make this inference consists of ^{14}C controlled relative sea level (RSL) histories in the age range 0-18 kyr B.P. (before present). It is of course very well known that such data depend not only upon the history of deglaciation but also upon the rheology of the planetary mantle. In fact, the dependence upon the latter influence is known to be so dominant at sites which were actually covered by ice and for times subsequent to the end of deglaciation that the RSL data provide tight constraints upon the radial variation of mantle viscosity [e.g., Haskell, 1935; McConnell, 1968; Peltier, 1982]. However, the past decade of research on the "forward modeling" of the glacial isostatic adjustment process (e.g., Peltier, [1974, 1976, 1985] and as recently reviewed by Peltier [1989]) has very clearly established that all of the RSL, free air gravity, and Earth rotation constraints are very well fit with a relatively simple model of the radial viscoelastic structure. With the elastic component of this structure determined by the results of body wave and free oscillation seismology (i.e., model 1066B of Gilbert and Dziewonski [1976] or PREM of Dziewonski and Anderson [1981]), most data have been shown to be very well reconciled by a model with an elastic lithosphere of thickness 120 km, an upper mantle with a viscosity

of 10^{21} Pa s and a lower mantle with a viscosity of $2-4 \times 10^{21}$ Pa s. This inference was based upon solutions of the forward problem in which an a priori model of the deglaciation history essentially tabulated by *Peltier and Andrews* [1976] was employed. Although this tabulated model (called ICE-1 by Peltier and Andrews) was later modified by *Wu and Peltier* [1983] to include an Antarctic component (then called ICE-2), the timing of which was further modified following arguments of *Peltier* [1988a], these modifications have not lead to any substantial required modification of the radial viscoelastic structure.

From both a geophysical and a paleoclimatological perspective, it is in fact useful to view the problem of glacial isostatic adjustment as a nonlinear inverse problem in which one hopes to infer from the data not only the internal viscoelastic structure of the planet but also the history of deglaciation to which its surface was subject. For the most part our effort to date has been focused upon the first step in the iterative solution of this inverse problem. Namely, the problem: given the deglaciation history, determine the radial viscoelastic structure. It is upon the second step in this iterative process, namely, the problem of how to refine the deglaciation history once an acceptable radial viscoelastic structure has been determined, that the present paper is focused. Although the earlier paper of *Wu and Peltier* [1983] employed similar methods to those to be employed here, that analysis was carried forward at significantly lower spatial resolution and used a very small number of RSL curves as constraints. The differences between the ICE-1 model of Peltier and Andrews and the ICE-2 model of Wu and Peltier in the northern hemisphere are therefore minor. As we will see, the same will not be the case for the new high-resolution ICE-3G model that will follow from the analyses to be presented here. An assessment of the uniqueness of the viscoelastic Earth structure and the deglaciation histories inferred from these analyses is currently ongoing using the formal theory of *Peltier* [1976] and *Mitrovica and Peltier* [1990].

The plan of this paper is as follows. In the next section we shall review the theoretical structure of the gravitationally self-consistent theoretical model that is employed to predict postglacial RSL histories given a radial viscoelastic structure and a deglaciation history. In section 3 the constraints that will be invoked to constrain the parameters of the deglaciation model are discussed. In section 4 the new model ICE-3G is discussed in detail and compared to models previously derived by other means with respect to several critical characteristics. Our conclusions are presented in section 5.

THEORETICAL BACKGROUND

This section briefly reviews the mathematical apparatus to be employed in the construction of ICE-3G. This apparatus was originally developed and has been described in greater detail elsewhere (see *Peltier* [1989] for a very recent review).

Construction of the Sea Level Equation

To compute the response of the Earth to a global deglaciation event, both a detailed spatio-temporal model of ice thickness change and a viscoelastic model of the planetary interior are required. An appropriate linearly viscoelastic Earth model is completely determined by the viscosity profile of the mantle $\nu(r)$ coupled with the seismically determined profiles of density $\rho(r)$ and elastic Lamé parameters $\lambda(r)$ and $\mu(r)$. From these profiles appropriate Green's functions $G(r, t)$ for the response of the Earth to applied surface loads can be constructed [*Peltier*, 1974]. As

discussed in the introduction, for the purposes of the present paper the radial viscoelastic structure of the planet will be assumed fixed to that previously shown to fit the totality of the isostatic adjustment constraints. The deglaciation history is best described by a function $L_I(r, t)$ that specifies the variation in space and time of ice thickness on the Earth's surface. The careful inference of an appropriate $L_I(r, t)$ for the past 18,000 radiocarbon years of Earth history, based primarily upon fits of the model to relative sea level histories, is the main purpose of the analysis to be described here.

As the ice sheets retreat, meltwater is added instantaneously (for our purpose) to the oceans and it must be distributed over them in such a way that the ocean's surface remains a surface of constant gravitational potential. However, this addition of meltwater is only one of the two effects which a melting event causes. The second effect is the geopotential change induced at the Earth's surface by the dynamical adjustment of the interior of the planet due to the unloading of the ice sheets and the subsequent loading of the ocean basins. The objective of the theory of postglacial relative sea level change is to compute local bathymetry changes (S) due to the melting of the major ice sheets, because it is such changes that the radiocarbon-controlled relative sea level histories record. To compute this change, we must first (following *Farrell and Clark* [1976], *Clark et al.* [1978], and *Peltier et al.* [1978]) compute the change of potential Φ on the ocean surface at point r and time t produced by a melting event L_I which in turn produces a bathymetry change S as

$$\Phi(r, t) = \rho_I L_I * \phi + \rho_w S * \phi \tag{1}$$

in which $*_I$ and $*_o$ indicate convolutions from time $t = -\infty$ until present time t over the ice and over the oceans, respectively, where ρ_I and ρ_w are the densities of ice and water, respectively, and where ϕ is the potential perturbation Green function [*Peltier and Andrews*, 1976] for the assumed known radially stratified viscoelastic model of the planetary interior. A melting event generates a change in ocean bathymetry (or sea level) which in turn produces a change in potential, but this causes a further change in sea level by the amount

$$S(r, t) = \frac{\Phi(r, t)}{g} + C \tag{2}$$

where g is the gravitational acceleration at the Earth's surface and C is a constant determined such as to ensure conservation of mass. To continue we must assume that the surface area of the oceans A_o remains constant. This assumption is of course incorrect since increasing sea level leads to coastal inundation; however, *Wu and Peltier* [1983] found that the overestimation of sea level rise due to this assumption was, as expected, minor, particularly in light of other errors as outlined in section 2.3. Since the mass loss of the ice sheets M_I must be equal to the mass gained by the oceans, we can write,

$$M_I = -\langle \rho_I L_I \rangle_I = -\langle \rho_w S \rangle_o \tag{3}$$

where the brackets $\langle \rangle_I$ and $\langle \rangle_o$ represent integrations over the ice sheets and oceans respectively. By substituting (1) into (3) we get

$$M_I = -\rho_w \langle \rho_I L_I * \phi + \rho_w S * \phi \rangle_o - \rho_w \langle C \rangle_o \tag{4}$$

Since C is a constant, $\langle C \rangle_o = CA_o$ where A_o is the total area of the ocean surface (assumed constant). Solving (4) for C and substituting into (2), the final form of the sea level equation

becomes

$$S = \rho_I \frac{\phi}{g} * L_I + \rho_w S * \frac{\phi}{g} - \frac{1}{A_o} \langle \rho_I L_I * \frac{\phi}{g} + \rho_w S * \frac{\phi}{g} \rangle - \frac{M_I(t)}{\rho_w A_o} \quad (5)$$

By constructing solutions to this integral equation, we can compare the predicted variations of sea level ($S(\mathbf{r}, t)$) to observed RSL histories.

Discretization of the sea level equation

In order to solve the integral equation (5) it must be discretized in both time and space in such a way as to allow numerical solution. To discretize (5) in time, we have elected to sample the temporal evolution of all fields at an interval of 1 kyr and hence the deglaciation history can be replaced by a sequence of step load removals (or occasionally additions) ΔL_i separated by $\Delta t = t_i - t_{i-1} = 1$ ky as

$$L_I(r', t) = \sum_{i=0}^P \delta L_i(r') H(t - t_i) \quad (6)$$

in which $H(t)$ is the Heaviside step function and P is the number of time intervals of duration Δt since deglaciation commenced. Before we can continue we must define the gravitational potential perturbation Green's function and expand it into its elastic and viscous parts [Peltier 1974; Peltier and Andrews, 1976] as

$$\frac{\phi^H}{g} = G^H = G^E + G^{H,V} = \frac{a}{M_e} \sum_{n=0}^{\infty} \left[(1 + k_n^E - h_n^E) \delta(t) + k_n^V(t) - h_n^V(t) \right] \quad (7)$$

in which h_n^E , (k_n^E) and h_n^V , (k_n^V) are the elastic and viscous components of the usual surface load Love numbers [see Peltier, 1974], and M_e and a are the mass and radius of the Earth, respectively. The sea level equation (4) may now be written as:

$$S(\mathbf{r}, t) = \iint \rho_I L_I(r', t) G^E(r') d^2 r' + \iint \rho_w S(r', t) G^E(r-r') d^2 r' + \rho_I \sum_{i=0}^P P_i \iint \delta L_i(r') G^{H,V}(r-r', t-t_i) d^2 r' + \rho_w \sum_{i=0}^P \iint \delta S_i(r') G^{H,V}(r-r', t-t_i) d^2 r' - C(t) \quad (8)$$

where δS_i is the increment in local bathymetry and the function $C(t)$ is given as

$$C(t) = \frac{1}{A_o} \left[\iint \rho_I L_I(r', t) G^E(r-r') d^2 r' + \iint \rho_w S(r', t) G^E(r-r') d^2 r' + \iint \rho_I \delta L_i(r') G^{H,V}(r-r', t-t_i) d^2 r' \right] + \iint \rho_w \delta S_i(r') G^{H,V}(r-r', t-t_i) d^2 r' + S_{EUS}(t) \quad (9)$$

where the 'eustatic' water rise is just

$$S_{EUS}(t) = \frac{\rho_I}{\rho_w A_o} \iint L_I(r', t) d^2 r' \quad (10)$$

To discretize the spatial dependence in (8), the Earth's surface is divided into a number of finite geometric elements. The "active" elements cover all of the ocean surface and those regions of the continents where glaciation and deglaciation actually took place. In the construction of ICE-2, Wu and Peltier [1983] covered the glaciated areas by 236 elements, all equally spaced with 5° longitude or latitude separating the centroids of the adjacent elements. For present purposes this previously employed coarse discretization has been abandoned in favour of a much finer grid with an average separation of 2° between centroids of adjacent elements but with elements now spaced so that the gaps and overlaps in the original discretization (discussed in section 2.3) are minimized. The 808 elements of this new ice grid for the northern and southern hemispheres are shown in Figure 1. The grid which covers the ocean basins has similarly been substantially modified for the present work from the original 470 nonuniformly spaced elements to the new ocean grid which has 557 elements positioned so that the continental outlines are more sharply delineated. This new ocean grid is illustrated in Figure 2.

Completing the discretization of (8), the sea level change S_{ip} at the centroid of the i th element located at \mathbf{r}_i due to a change in the j th active element (E_j) at time p may be computed as:

$$S_{ip} = \rho_w G_{ij}^E S_{jp} + \rho_I G_{ij}^E I_{jp} + \rho_w G_{ijp}^{H,V} \delta S_{jt} + \rho_I G_{ijp}^{H,V} \delta I_{jt} - \frac{\rho_I}{\rho_w A_o} E_j I_{jp} - \frac{E_{\kappa}}{A_o} \left(\rho_w G_{\kappa j}^E S_{jp} + \rho_I G_{\kappa j}^E I_{jp} + \rho_w G_{\kappa p}^{H,V} \delta S_{jt} + \rho_I G_{\kappa p}^{H,V} \delta I_{jt} \right) \quad (11)$$

where for terms involving S_{jp} and δS_{jp} , j is summed over the finite elements in the oceans from 1 to N ($= 557$), for terms involving I_{jp} and δI_{jp} , j is summed over the elements in the ice sheets from 1 to M ($= 808$) and for terms involving δS_{jp} and δI_{jp} , p is summed from 1 to P ($= 22$) where P is the number of time intervals ($\Delta t = 1$ kyr)

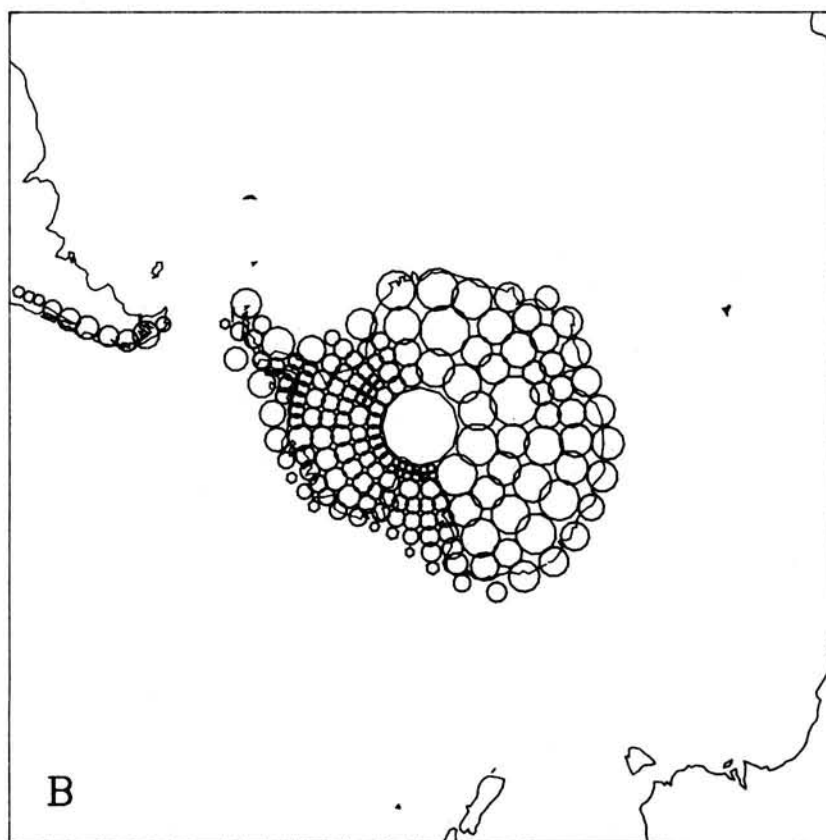
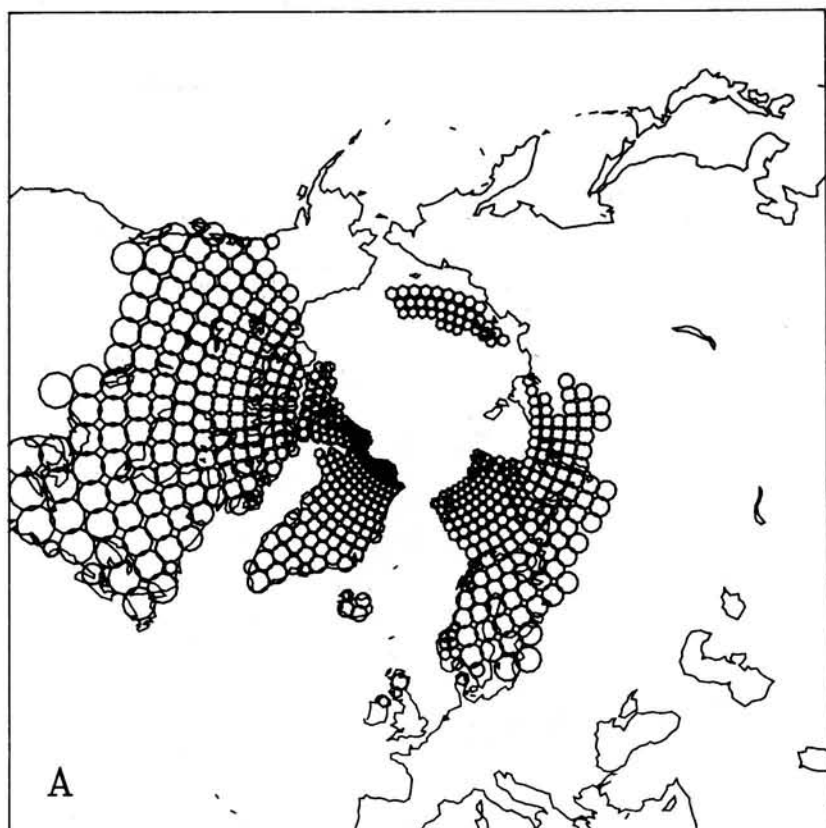


Fig. 1. Finite element grid for ice cover. (a) Northern and (b) Southern Hemispheres.

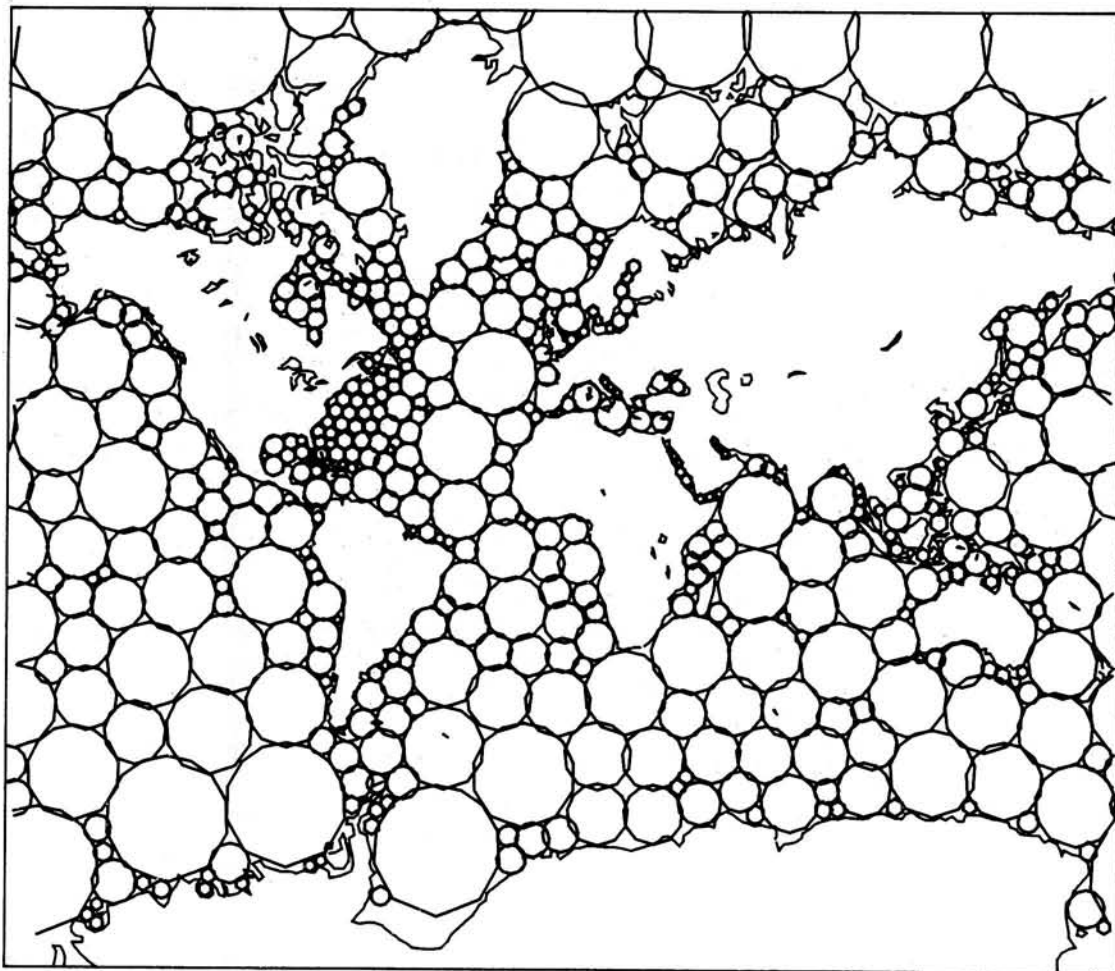


Fig. 2. Finite element grid for ocean basins. Note the fine gridding along the coasts.

since deglaciation commenced. The matrices are defined as:

$$S_{ip} = S(r_i, t_p),$$

total relative sea level change at r_i by time t_p ;

$$I_{ip} = L_i(r_i, t_p),$$

total thickness of ice removed at r_i by time t_p ; δ

$$\delta S_{ip} = \delta S(r_i, t_p) = S_{ip} - S_i(p-1),$$

increment of seawater thickness at r_i for time t_p ;

$$\delta I_{ip} = \delta L_p(r_i) = I_{ip} - I_i(p-1),$$

increment of ice thickness at r_i for time t_p ;

$$G_{ij}^E = \int_{E_j} \int G^E(r-r') d^2 r',$$

the elastic response at r_i due to the j^{th} finite element;

$$G_{ip}^{H,V} = \int_{E_j} \int G^{H,V}(r-r', t_p-t_i) d^2 r',$$

the viscous response at r_i for time t_p due to Heaviside loading of the j^{th} element at time t_i .

The response at the centroid of the i^{th} element due to loading of the j^{th} element depends not only on the separation $r_i - r_j$ but also on the shape of the elements. To reduce the computational requirements of computing the interaction matrices, the shape dependence was suppressed by replacing at the outset each rectangular finite element of the previous model [Wu and Peltier, 1983] by circular discs of equivalent area as explicitly shown in Figures 1 and 2.

The first estimate of the unknown S_{ip} is the solution which corresponds to a eustatic sea level rise; that is, a rise due to a uniform distribution of meltwater throughout the oceans. This eustatic rise can be computed as:

$$S_{ip}^1 = - \frac{\rho_i}{\rho_w} \cdot \frac{E_j}{A_o} \cdot I_{jp} \quad (12)$$

and the amount by which this first estimate fails to satisfy equation (11) is the residual S_{ip}^R . The eustatic estimate (12) is corrected by this residual amount to produce a second estimate

$$S_{ip}^2 = S_{ip}^1 + S_{ip}^R \quad (13)$$

and the process is continued until a converged solution is obtained (usually three or four iterations are sufficient).

Since RSL histories usually come in the form of data collected at coastal sites, we must use the solutions for the S_p values located at the centroid of each finite element to make accurate computations of the RSL history expected at the appropriate coastal location (see *Wu and Peltier* [1983] for details).

Limitations of the Finite Element Method

In the calculation of the changes in sea level undertaken in sections 2.1 and 2.2, we have had to make several assumptions and approximations, and it is to consideration of the importance of these that we shall now turn. We have assumed that the surface area of the oceans does not increase as the ice sheets melt and we have implicitly assumed that isostatic equilibrium was established before any melting took place. As to the former effect, as previously mentioned, *Wu and Peltier* [1983] concluded that the amount of the overestimate of sea level rise was very small (especially when compared to other sources of errors). In so far as the latter effect is concerned, if isostatic equilibrium did prevail initially then we could predict RSL histories with only a knowledge of ice load removal. *Wu and Peltier* [1983] discussed this assumption in detail and found only minor differences between the response assuming initial isostatic equilibrium and the response calculated with a realistic saw-tooth glaciation deglaciation loading prehistory inferred from $\delta^{18}O$ data from deep-sea sedimentary cores (see section 3.2). These minor differences are within the uncertainty of the RSL measurements themselves and for present purposes we shall henceforth ignore the effects of initial isostatic disequilibrium.

The main approximations made here have been in the discretizations assumed for the temporal and the spatial variability of the unknown fields. The temporal variability has been discretized by evolving all fields at time intervals of $\Delta t = 1$ kyr. Since the deglaciation event studied here took 18 kyr to complete (on the ^{14}C time scale), the approximation is fairly good for the overall description of the ice sheets but will not describe any minor advances or retreats on a time scale less than 1 kyr, such as those across the Hudson Strait (*J. Stravers*, personal communication, 1986).

A much more serious problem concerns the approximation used in the spatial discretization. For ICE-2, *Wu and Peltier* [1983] employed 236 finite rectangular elements to define the ice sheets and 470 to define the ocean basins, but the coarse $5^\circ \times 5^\circ$ ice grid of ICE-2 caused problems of spatial resolution. For example, over the Canadian Maritimes there was only a single element and the actual complex deglaciation history in this region [e.g., *Quinlan*, 1981] could therefore not possibly be accurately represented. In constructing our new ICE-3G model in the present work the ice grid was refined to approximately $2^\circ \times 2^\circ$ resolution and in regions where RSL data is abundant to approximately $1^\circ \times 1^\circ$. This refinement required the number of finite elements to be increased to 808 (as mentioned previously) which now allows for a far more accurate representation of the variations of ice sheet thickness. A second problem, also mentioned previously, is that which arises because the elements were originally rectangular and subsequently represented by equivalent circular discs. A consequence of this was that there were inevitably regions in which two discs overlapped and others which were not covered at all. Here we have abandoned the rectangular element mapping and instead use circular disc elements from the onset. The location and size of the discs are adjusted so that the overlaps and gaps are

minimized (refer to Figures 1 and 2). Finally, the continental coastlines were not well represented by the previous ocean grid, with land masses such as the British Isles, Madagascar, New Zealand, Iceland and Central America considered part of the ocean. The new ocean grid was carefully reconstructed with 557 finite elements so that the coastlines are accurately defined, even around large islands. In the course of further analyses (*J.X. Mitrovica and W.R. Peltier*, A complete formulation for the inversion of post-glacial rebound data: Resolving power analysis, submitted to *Geophysical Journal*, 1990b) we have abandoned the finite element technique entirely and use spherical harmonics to represent the spatial fields. The solutions to be presented in the present paper are essentially identical to those delivered by the spherical harmonic techniques when expansions are truncated at degree and order 128.

CONSTRAINING THE MODEL OF DEGLACIATION

Probably the most obvious constraint imposed on any model of deglaciation is that provided by geological evidence in the form of glacial tills, striations, moraines, and a myriad of other features which indicate that an ice sheet once covered the land. Predictions of ice extent from the analyses to be presented here will be compared to the most recent maps based on such data [e.g., *Dyke and Prest*, 1987a, b, *Grosswald*, 1980] in section 4. Here, constraints on the model imposed by relative sea level (RSL) histories and $\delta^{18}O$ data from deep-sea cores will also be discussed. The former offer a means with which to estimate changes in local ice thickness and the latter a basis on which to estimate changes in global ice volume.

Implementation of the Constraints Imposed by RSL Data

Using the previously discussed glacial isostatic rebound theory, a predicted sea level history can be computed for any location one wishes. By comparing the predicted sea level history to observed RSL data at every ice-covered site and one far-field site (as shown in Figure 3) the final form of ICE-3G was determined. If, for example, the predicted sea level elevation was lower than the observed elevation, the ice load in that region was either increased in thickness or its melting delayed. Careful analysis of the RSL data for the target site and surrounding areas then indicates which particular combination of increased thickness and delay of melting is required. Predictions from this new ice model are again compared to the RSL data base and so on. After 19 such iterations on the global model, we settled on the final form of ICE-3G that is tabulated in Appendix A1. The implications of this final form of the deglaciation model will be discussed at length in section 4. The original sources for the RSL data used to constrain the iteration process are listed in future paper (*A.M. Tushingham and W.R. Peltier*, Validation of the ICE-3G model of Würm-Wisconsin deglaciation using a global data base of relative sea level histories, submitted to *Journal of Geophysical Research*, 1990).

Figure 4 displays a sample of predicted sea level curves for six North American and six European sites for both the old ICE-2 model and the new ICE-3G model which allows an initial assessment of the improvement achieved with the newly constructed deglaciation history. The ICE-3G predicted sea level curves are very close to the observed data at all sites and fits to the data delivered with the ICE-2 model are markedly inferior. The extent to which this is true for all available sea level data will constitute a true measure of the global improvement that has been achieved with the newly constructed model in the ice covered

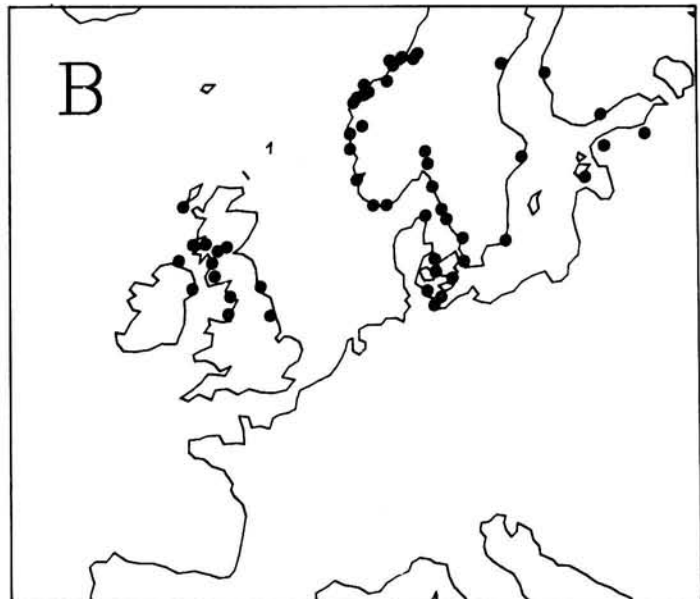
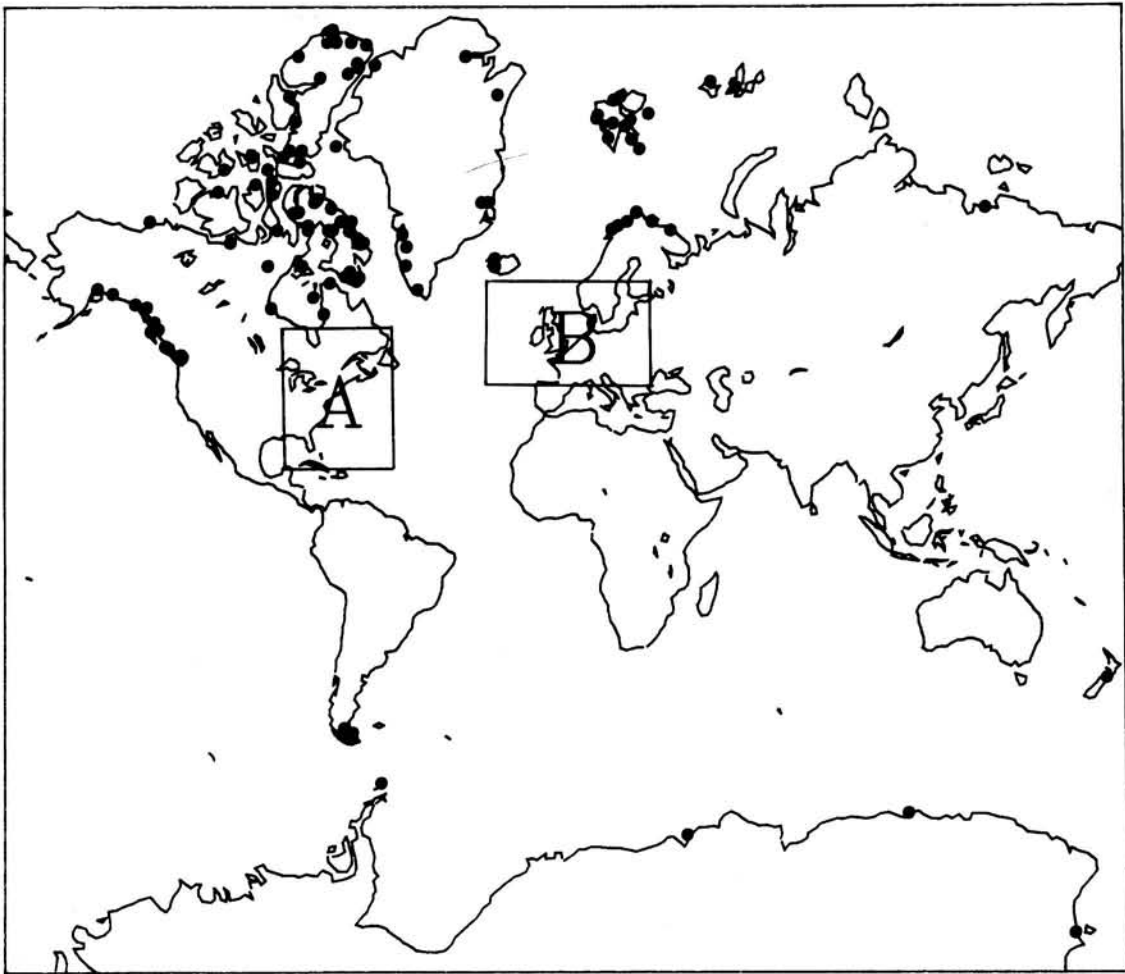


Fig. 3. RSL site location map. For eastern North America and Europe refer to enlargements A and B, respectively. The circles represent sites employed in constructing ICE-3G.

regions. At most of the sites from which data are available ICE-3G predicted curves are indeed favored over those of ICE-2. To quantify the extent of the improvement, a global measure of the differences between the predicted curves and the observed data points was computed by using the following global measure of the misfit, or "variance":

$$\sigma = \frac{1}{N} \sqrt{\sum_{i=1}^N (H_i^p(t) - H_i^o(t))^2}$$

where $H_i^p(t)$ and $H_i^o(t)$ are the predicted and observed sea level heights at time t , respectively, and N is the number of RSL data points in the global data set. The uncertainty in the observed age Δt was incorporated into the variance by varying the time from $t - \Delta t$ to $t + \Delta t$ and finding the minimum value of the height difference. The uncertainty in the observed height $\Delta H_i^o(t)$ was employed to determine the minimum variance possible given the uncertainty in the data set by using

$$\sigma_{\min} = \frac{1}{N} \sqrt{\sum_{i=1}^N (2\Delta H_i^o(t))^2}$$

The factor of 2 incorporates the range of uncertainty between $-\Delta H_i^o(t)$ and $+\Delta H_i^o(t)$. Table 1 summarizes the variance calculation for the RSL data set employed in the construction of ICE-3G by region as well as globally. With the exception of the Atlantic, Indian and Southern Oceans region, all variances are smaller for the ICE-3G model than for the ICE-2 model. In fact, the ICE-3G global variance is smaller than the minimum variance based on the uncertainties of the actual RSL data, but this is not true for the ICE-2 global variance. The problem arising in the Atlantic, Indian and Southern Oceans region is due to one very poorly fitting site in Antarctica, namely McMurdo Sound, which has 8 of the 16 data points in this region. The remaining three Antarctic sites plus a Patagonian site have RSL histories which agree quite well with the predicted RSL curves of ICE-3G, as we shall see.

The RSL curves in Figure 4 and the variance summary in Table 1 both demonstrate the marked improvement of the predicted sea level histories in the ice covered areas.

Constraints Imposed by $\delta^{18}O$ Data

Although the large number and wide distribution of RSL sites allow detailed local adjustments to be made to the ice model independent of any other constraint, more confidence in the resulting model will be warranted if its predictions also agree with observations that have not themselves been employed in constructing it. Previous ice sheet reconstructions have been based on single data types and rarely quantitatively compared to other constraints. Here we shall compare the new ice sheet reconstruction to a constraint not normally employed in such work, leaving to the companion paper its detailed verification against a large set of relative sea level data from sites outside the ice covered regions. For example, the sea level calculation can quite easily be employed to predict the magnitude of the maximum sea level rise since 18,000 years B.P. as a function of geographic location, and this is precisely the parameter which oxygen isotope analyses can be invoked to determine. The variations in the oxygen isotopic abundance ratio ($^{18}O/^{16}O$) as measured in marine microfossils were first employed as indicators of paleo-temperatures in the oceans by Epstein *et al.* [1951] and Emiliani [1955], based on a proposal by Urey (1947). Emiliani modified Epstein *et al.*'s equation from which paleo-temperatures were derived to

$$T = 16.5 - 4.3 (\delta^{18}O - A) + 0.14 (\delta^{18}O - A)^2$$

where $\delta^{18}O$ is the difference between the $^{18}O/^{16}O$ content of the sample analysed and a standard carbonate and is defined as

$$\delta^{18}O = 1000 \left(\frac{(^{18}O/^{16}O)_{\text{sample}} - (^{18}O/^{16}O)_{\text{standard}}}{(^{18}O/^{16}O)_{\text{standard}}} \right)$$

The term A represents the difference between the isotopic composition of ancient seawater in which the fossil analyzed had lived and the average for modern seawater, and was introduced by Emiliani to correct for the changing isotopic composition during each glacial-interglacial cycle. Emiliani was able to estimate the change in surface water temperature of the Caribbean Sea to be

TABLE 1. Variance Statistics for RSL Sites Used in the Construction of ICE-3G

Region	Number Sites	Number of Data	Variance		
			ICE-2	ICE-3	Minimum
Arctic Canada and Greenland	69	365	1.65	0.75	1.09
Northern Europe	73	397	1.91	0.61	0.59
Eastern North America	25	152	2.58	1.32	1.71
Southern Europe	2	11	5.33	1.93	1.41
Atlantic, Indian and Southern Oceans	5	16	1.32	3.63	0.73
Pacific Ocean	18	79	3.95	2.72	1.26
Global	192	1020	1.07	0.47	0.53

Sites which are ICE-2 preferred = 32 neutral = 38 ICE-3 preferred = 122. ICE-2 fits 2.60% of the sites within the minimum variance and 48.4% within twice the minimum variance. ICE-3G fits 54.7% of the sites within the minimum variance and 80.7% within twice the minimum variance.

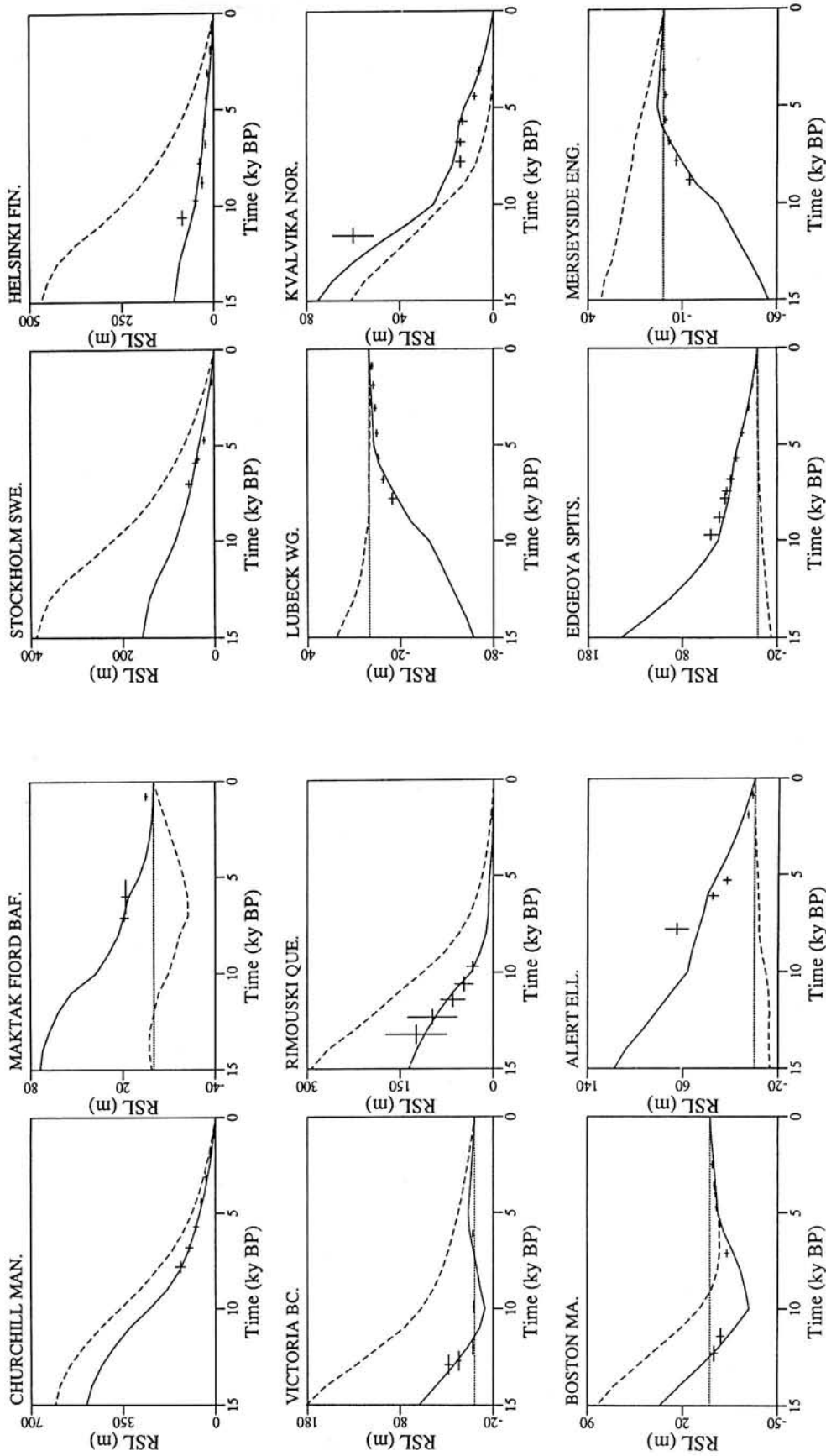


Fig. 4. (a) Sample RSL predictions at North American sites. The solid and dashed curves represent ICE-3G and ICE-2 predicted curves, respectively.

The ages of the samples have been converted into sidereal years. (b) Sample RSL predictions at European sites.

about 6°C, but *Olausson* [1965] doubted that tropical temperature changes could have been that large.

Shackleton [1967], attempting to resolve this controversy, analyzed the isotopic composition of benthonic foraminifera, as opposed to planktonic species, so as to minimize the influence of the temperature change. He inferred that most of the $\delta^{18}\text{O}$ signal in the foraminifera was due to changes in the isotopic composition of seawater which relates to changes in global ice volume, and that temperature changes were a secondary effect. Further he noted that the record of ocean isotopic composition change was of even more value than was a temperature record in view of its direct relationship to global ice volume and hence to sea level. For example, as the ice sheets grew, ^{16}O was preferentially removed from the oceans and sequestered in the ice sheets. The $^{18}\text{O}/^{16}\text{O}$ ratio therefore increased in the oceans and oxygen subsequently absorbed into marine microorganisms had this larger isotopic ratio. The larger ratios thus correspond to glacial maxima and the smaller ratios to interglacial periods.

The oxygen-isotope analysis is, however, complicated by disequilibrium effects and other uncertainties. *Shackleton and Opdyke* [1973] and *Vergnaud-Grazzini* [1976] suggested that some planktonic species are naturally depleted in ^{18}O , while *Emiliani* [1954] and *Shackleton and Vincent* [1978] stressed that the depth habitat of the organism (i.e., above or below the thermocline) would affect the isotopic concentration as would the seasonal growing variation. The controversy over the low $\delta^{18}\text{O}$ meltwater spike [*Berger et al.*, 1977; *Jones and Ruddiman*, 1982] adds further uncertainty to an already variable isotopic record. Other uncertainties include sedimentary accumulation changes [*Shackleton and Opdyke*, 1973], selective dissolution [*Berger and Killingley*, 1977], and most importantly changes in ocean mixing and hence deep-ocean temperature [*Shackleton and Opdyke*, 1976; *Bowen*, 1978]. Both ocean mixing and deep-ocean temperature are dependent on the polar downwelling zones of cold water, and these

zones have changed substantially since the glacial maxima. Comprehensive reviews of oxygen-isotope analysis have been recently compiled by *Mix and Ruddiman* [1984] and *Mix* [1987].

Shackleton and Opdyke [1973] were the first to determine a sea level curve directly from $\delta^{18}\text{O}$ data. They examined the upper 230 cm of the piston core V28-238 recovered from a depth of 3120 m on the Solomon Plateau in the western Pacific Ocean by sampling the core at 5-cm intervals and selecting *Globigerinoides sacculifera* as a representative planktonic foraminiferal species. Using a time scale derived from the position of the Brunhes-Matuyama magnetic reversal boundary and the assumption of uniform sedimentary accumulation rate (which appears to be valid for this core), they constructed a sea level history for the past 130,000 years. Their curve agreed with the work of *Veeh and Chappell* [1970] on the coral terraces of Huon Peninsula, Papua New Guinea. From this curve they deduced the local sea level rise since the last glacial maximum to be 120 m. This value is clearly a strong constraint on the maximum global ice volume in ICE-3G. More recently, *Chappell and Shackleton* [1986] derived a second related estimate of maximum sea level rise. They analyzed benthic *Uvigerina senticososa* found in the sediments of the East Pacific core V19-30 which was first examined by *Shackleton et al.* [1983]. Defining a time scale from orbital data they estimated the local sea level rise after correcting for local uplift to be about 130 m. Their sea level curve, at least for the last 20,000 years, agrees with the curve estimated by *Chappell* [1983] from the radiocarbon-determined ages and elevations of the coral terraces on the Huon Peninsula (refer to Figure 5). A maximum sea level rise in the western Pacific of between 120 and 130 m may then be employed as a constraint on the maximum ice volume of ICE-3G. The use of $\delta^{18}\text{O}$ data in this manner to constrain a deglaciation model has apparently not been previously undertaken.

Working in the Caribbean Sea near Barbados, *Broecker et al.* [1968] and *Broecker and Van Donk* [1970] studied the ages and

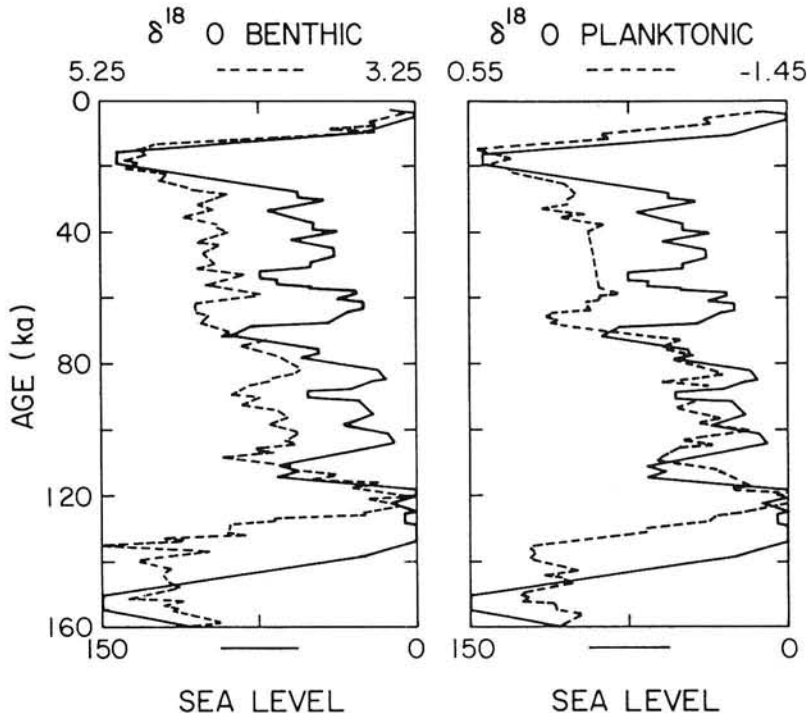


Fig. 5. Comparison between sea level (solid) and $\delta^{18}\text{O}$ data (dashed) for benthic and planktonic microorganisms. Note the excellent agreement for at least the last 20 kyr [from *Mix*, 1987].

elevations of the Barbadian coral reefs and deduced a value for the maximum sea level rise in the southern Caribbean to be between 90 and 100 m. More recent work by *Fairbanks* [1989] and *Bard et al.* [1990] has revised this estimate to a value near 120 m and therefore closer to that from the Huon Peninsula. It is obviously very important that any sea level calculation not only correctly predict the value of the net "eustatic" sea level rise but also its variation with geographic position, a variation which appears to be required by the discrepancy between the total sea level rise estimated on the basis of western Pacific and Caribbean data. The term "eustatic" sea level rise has been widely and inaccurately adopted to describe the response of the oceans to the influx of meltwater caused by ice sheet disintegration, and it is usually taken to imply that meltwater is distributed equally to all parts of the world's oceans as the ice melts. However, as mentioned previously, meltwater is in fact distributed in such a way that the surface of the ocean is maintained as an equipotential surface at all times. The differences between the two ranges (observed by *Fairbanks* and *Bard et al.* and by *Chappell* and *Shackleton*) might be interpreted as being directly due to this phenomenon.

The deglaciation model ICE-2 led to a maximum sea level rise in the western Pacific of 97 m which is 20%-25% lower than the range discussed above, while the ICE-3G value is 115 m which is only 4%-12% too low. In fact the estimate of 130 metres by

Chappell and *Shackleton* may have assumed a smaller temperature effect than is reasonable, which could reduce the maximum sea level rise estimate by up to 15 metres to our value of 115 metres (*J. T. Andrews*, personal communication, 1988). Alternatively, and more probably, we may still be missing ice because regions that have been assumed to be ice free in the new model (such as eastern Siberia) may in fact have been significantly glaciated. In the southern Caribbean, ICE-2 predicted only 87 m of sea level rise, but ICE-3G now predicts 103 m. The upper value is again about 17 m lower than the value of 120 m that has been deduced by *Fairbanks* [1989]. Figure 6 displays total sea level rise predictions for ICE-2 and ICE-3G and clearly illustrates the increase in this important quantity delivered by the new model.

In order to achieve these markedly improved estimates, three additional ice sheets were added to those in the original ICE-2 compilation. Whereas most of the original ice sheets were confined in thickness and extent by the RSL data set, along the north coast of the Soviet Union almost no such data exist. The Barents Sea, Kara Sea, and East Siberian Sea Ice Sheets were, nevertheless, included in the model (evidence for these ice sheets will be discussed in section 4.2) and subsequently added 16 m to the total sea level rise estimate, as demonstrated in Table 2. This table divides the total sea level rise at the location of core V28-238 into the components due to each of the individual ice sheets.

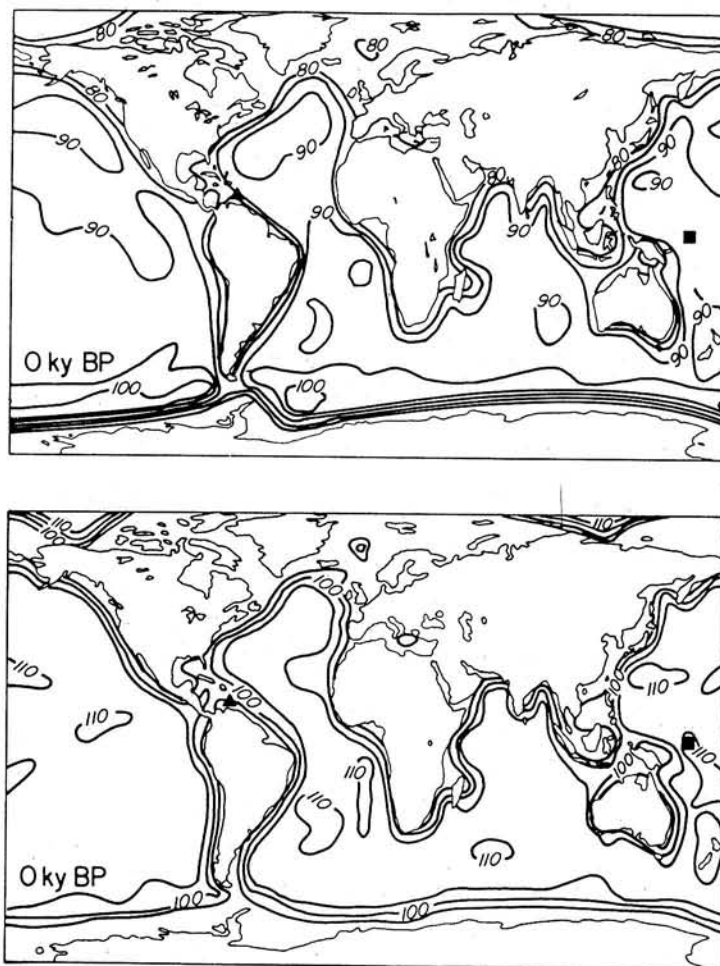


Fig. 6. The total sea level rise predicted by the (top) ICE-2 model and the (bottom) ICE-3G model. Contours are every 5 m. The square indicates the location of deep-sea core V28-238 and the triangle the location of the Barbadian coral reefs.

TABLE 2. Component of Sea-Level Rise Due to Each Ice Sheet

Ice Sheet	Maximum Volume, m ³	Maximum Mass, kg	Present Volume, m ³	Present Mass, kg	Ocean Rise, m
Imuitian	0.99E15	0.89E18	0.34E14	0.31E17	3
Laurentide	0.21E17	0.19E20	0.35E14	0.31E17	55
Greenland	0.55E16	0.49E19	0.30E16	0.27E19	6
Fennoscandian	0.29E16	0.26E19	0.00E00	0.00E00	8
Barents Sea	0.22E16	0.20E19	0.86E13	0.77E16	6
Kara Sea	0.26E16	0.24E19	0.00E00	0.00E00	7
East Siberian Sea	0.11E16	0.99E18	0.00E00	0.00E00	3
Iceland	0.20E15	0.18E18	0.00E00	0.00E00	1
Scotland	0.96E14	0.86E17	0.00E00	0.00E00	0
Patagonian	0.18E15	0.16E18	0.00E00	0.00E00	0
Antarctic	0.35E17	0.32E20	0.26E17	0.23E20	26
Total	0.72E17	0.65E20	0.29E17	0.26E20	115
			Subsequent Ocean Rise		76

The detailed changes in sea level during the last 18,000 years predicted with the deglaciation history ICE-3G are illustrated in Figure 7. Upon reviewing this sequence of maps, it will be seen that sea level rose rapidly until about 7000 years B.P., then leveled off to reach a maximum at 5000 years BP, and finally fell in the equatorial ocean by a small amount to its present level. The reason for the slow fall of sea level predicted for the equatorial oceans at present is discussed in detail in a forthcoming article by J.X. Mitrovica and W.R. Peltier (1990) using the newly developed spherical harmonics solution to the sea level equation. Put simply, sea level is caused to fall in the equatorial ocean after deglaciation is complete because postglacial rebound of the crust in the polar regions increases the gravitation attraction of the water to this region, causing it to flow from the equatorial to the polar oceans.

Overall, ICE-3G provides rather accurate RSL predictions at the vast majority of ice-covered sites and, to within about 15%, agrees with the total sea level rise determined by $\delta^{18}\text{O}$ and coral terrace data in the western Pacific and coral terrace data in the southern Caribbean. This residual 15% error is easily explained by the basis of new constraints that are now forthcoming on the relation between the radiocarbon and sidereal time scales [Bard *et al.*, 1990]. They will be integrated into a further refinement of the deglaciation history in a later publication.

DETAILED DISCUSSION OF THE DEGLACIATION HISTORY ICE-3G

The characteristics of the new deglaciation history that we have derived for the last 18,000 radiocarbon years will be discussed separately for North America, Europe and Asia, and Antarctica in the next three sub-sections.

The Deglaciation of North America

Prior to 1943, it was generally believed that the Laurentide Ice Sheet was the composite of three ice domes located over

Keewatin, Northern Quebec, and Northern Ontario [e.g., Tyrrell, 1898]. However in the 1940s, Flint [1943, 1949] proposed, based upon gravity data defining the center of isostatic rebound and upon ice growth considerations, that the Laurentide Ice Sheet consisted of a single dome centred over Hudson Bay. He suggested that the ice sheet was nucleated in the mountains of northern Quebec then quickly expanded into the Hudson Bay basin which was in the direction of its precipitation source. The study of erratics and their sources and movements has only recently shown that serious problems could exist with Flint's monodomal ice model. Shilts *et al.* [1979] and Shilts (1980), studying distinctive Precambrian and Paleozoic erratics in Keewatin, suggested that it was highly improbable that ice ever flowed from Hudson Bay into Keewatin, and so concluded that there must have been two ice centers. Meanwhile, Andrews and Miller [1979], studying limestone erratics on Baffin Island, discovered a lack of probable flow lines from a single dome or even a pair of domes. They proposed that a third ice center in the Foxe Basin was necessary to explain the position of these erratics. Others have suggested that even more ice centers existed [Dyke *et al.* 1982; Andrews *et al.*, 1984; Shilts, 1984]. By including the isostatically light block on the west side of Hudson Bay [Hall, 1969], Dyke *et al.* [1982] concluded that the polydomal models could satisfy the gravitational isostatic data better than does the monodomal model, thus repudiating one of Flint's original arguments supporting the monodomal model.

The sea level changes during the last 18,000 years were clearly caused by the disintegration of the major ice sheets rather than by their growth. Denton and Hughes [1981], Hughes [1985], Shilts [1985], and others have modeled the disintegration of the Laurentide Ice Sheet, and Prest [1984] and Dyke and Prest [1987a, b] presented a series of paleogeographic maps which summarize the retreat of the North American ice sheets based on geological evidence. Here we will directly compare the glacial retreat maps of Dyke and Prest [1987a, b], subsequently referred to as the DPR maps, to the isochrones of the ICE-2 and ICE-3G models in order to further confirm the validity of the new deglaciation history. To

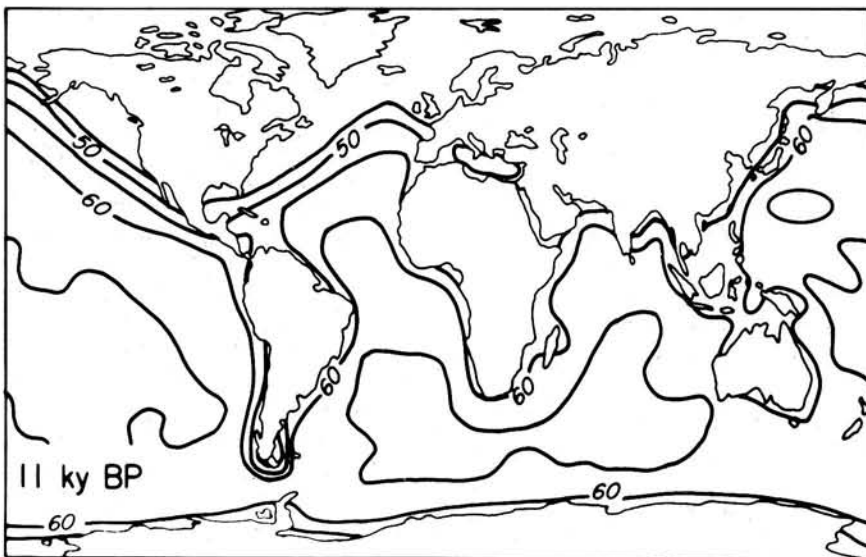
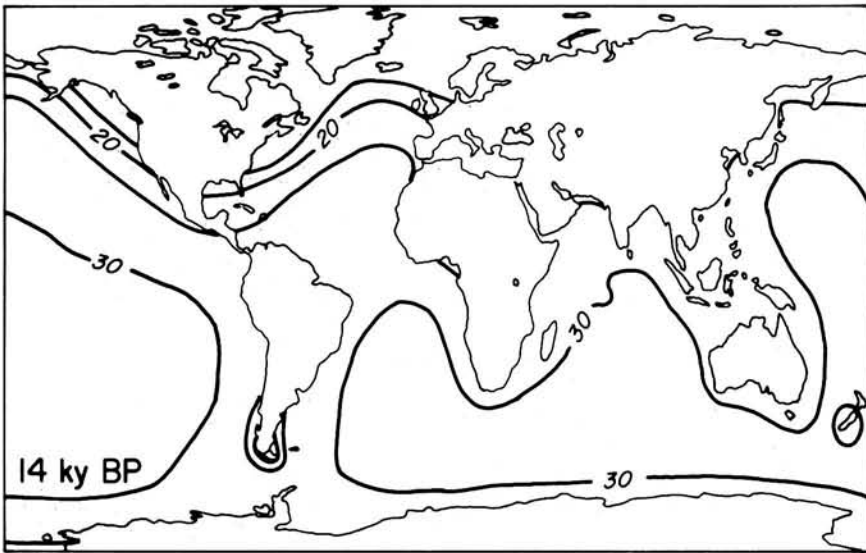
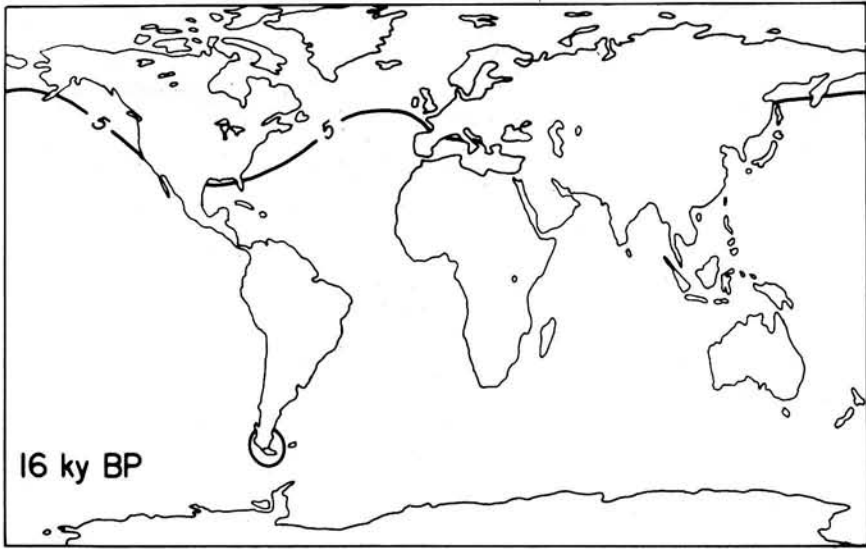


Fig. 7. Sea level rise maps. Contour interval is 5 m. This is a rapid increase in sea level from 16 to 5 kyr B.P. and then a small decrease due to the response of the ocean basins. (continued).

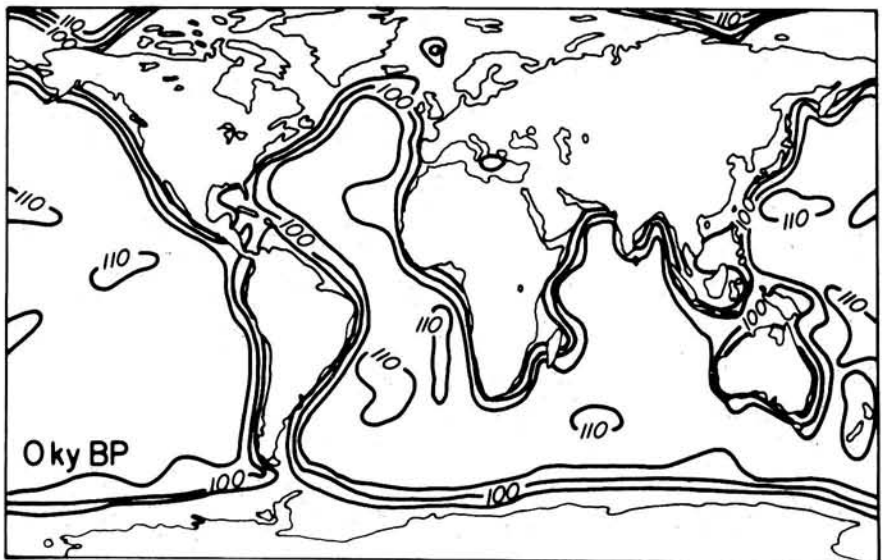
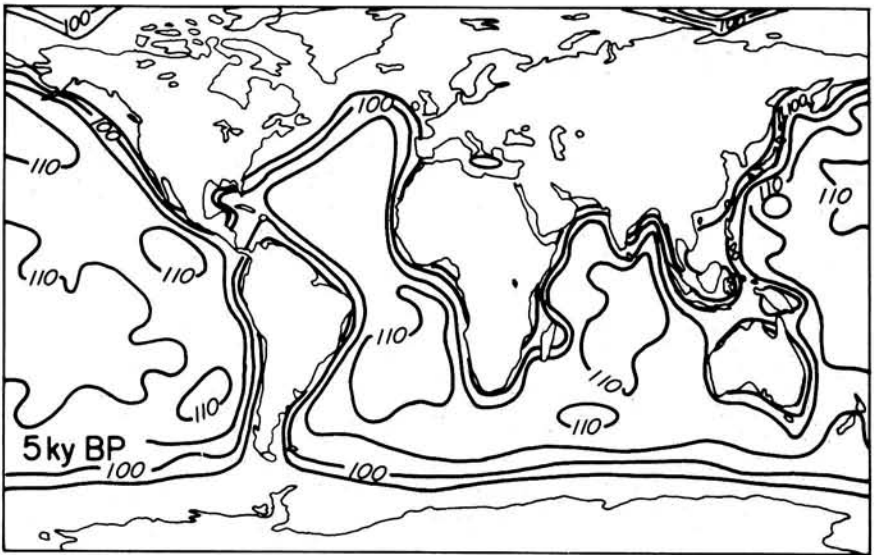
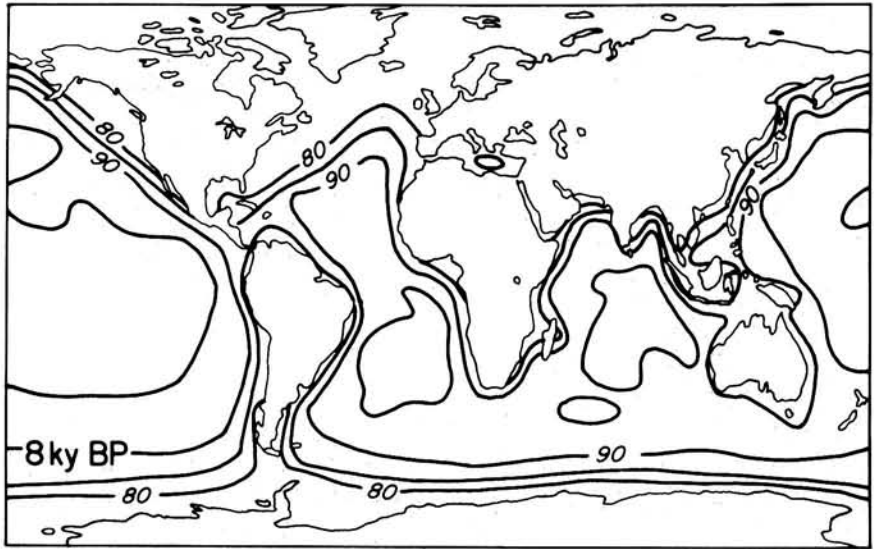


Fig. 7. (continued)

this end, the finite element ice grids of both ICE-2 and ICE-3G (refer to Figure 2) were overlain on the DPR maps and, since each grid element covers a large area, judgement was employed to assign to each grid element a date for total ice removal. This assigned date was then converted to sidereal years using the best data available [e.g., *Pearson et al.*, 1986; *Stuiver et al.*, 1986, to 8 kyr B.P.] so that it could be directly compared to the timing suggested by the ICE-2 and ICE-3G models by computing the variance

$$\sigma = \frac{1}{N} \sqrt{\sum_{i=1}^N (t_i^p - t_i^A)^2}$$

where t_i^p and t_i^A are the predicted and observed times of ice removal on the i^{th} grid element and N is the total number of grid elements. The minimum variance is defined as

$$\sigma_{\min} = \frac{1}{N} \sqrt{\sum_{i=1}^N (2\Delta t_i)^2}$$

where Δt_i is set at $\pm 4\%$ of t_i^A to allow for the uncertainty of radiocarbon dating with a minimum error of ± 500 years to reflect the difficulty in assigning a single date for an entire grid element. Table 3 displays the results of this analysis. For the Laurentide Ice Sheet the improvement achieved by the new iteration, as demonstrated by the ICE-2 to ICE-3G variance reduction, is dramatic and the ICE-3G variance is now well below the minimum variance. The DPR maps show the Parry Islands to be ice free, but ICE-3G has these islands covered by a westward extension of the main Innuitian Ice Sheet in order to allow better agreement between observed and predicted RSL histories for sites in this area (to be discussed later in this section). This means that the improvement for the Innuitian Ice Sheet is only minor.

The DPR maps based on geological data do not allow estimates of ice sheet thickness, but maps based on ice mechanical considerations [*Denton and Hughes*, 1981; *Hughes*, 1987] are able to provide estimates of this crucial parameter. The deglaciation history of ICE-3G will therefore be compared to Denton and Hughes' favored maximum ice sheet reconstruction (subsequently referred to as the DHMX model) and of course directly compared to the deglaciation history of ICE-2 and the DPR maps. The maximum ice cover for the DHMX model is shown in Figure 8, but the ice cover and deglaciation history for North America is illustrated in more detail by *Hughes* [1987].

TABLE 3. A Comparison Between Predicted Retreat Data and the DPR Maps

Ice Sheet	Ice Model	Number of Grid Elements	Variance	Minimum Variance
Innuitian	ICE-2	12	1.04	0.30
Innuitian	ICE-3G	59	0.41	0.16
Laurentide	ICE-2	86	0.29	0.12
Laurentide	ICE-3G	176	0.04	0.08

The deglaciation history of ICE-3G for North America and the rest of the Northern Hemisphere is summarized in a series of isopleth maps (Figure 9). One of the first differences between ICE-2 and ICE-3G to be noted and in fact the first change undertaken in the construction of ICE-3G (as suggested by J. Stravers, personal communication, 1986), is the earlier removal of ice from Hudson Strait and northern Hudson Bay (Southampton Island, Ungava Peninsula and Cape Tanfield; the places listed in parentheses are the RSL sites which have been employed to constrain the ice load in the particular region under discussion and the fits to the data at these sites are presented in Appendix B which is available on microfiche). The RSL predictions of ICE-3G were compared to the observations at these sites, any adjustments required were made accordingly, and the predictions were again compared. This iterative process was continued until the best possible fit to all the data in the region was achieved. ICE-2 had complete removal of ice in this area by 6000 years B.P. but ICE-3G had the ice removed by 8000 years BP. The new ICE-3G model now agrees with both the DPR maps and the DHMX model and provides excellent agreement with the RSL data in the area, as shown in Appendix B which presents a sequence of figures displaying the ICE-2 and ICE-3G predictions and the RSL data for each site. Concurrent with earlier removal of ice, the overall ice thicknesses over Hudson Bay and Keewatin were reduced from 3500 m to 3200 m over central Hudson Bay (Ottawa Island, Cape Henrietta Maria, and Churchill) and from 2000 m to 1800 m over Keewatin (Keewatin). These changes delivered excellent agreement with the observed RSL data. The thickness values are now much less than the 3500 meters over Hudson Bay and 3800 meters over Keewatin which the DHMX model proposes. Clearly, these excessive ice thicknesses would cause a much larger isostatic rebound than the RSL data indicates to have occurred when glacial maximum is assumed to occur at 18,000 years B.P.

On the east coast of Baffin Island, especially on the southern part of the island, large amounts of ice have been added. Whereas ICE-2 and the DHMX model propose less than 500 m of ice over the Home Bay area and actually predicted submergence at many sites in the region (Maktak, Narpain, Okoa and Neolukseak Fiords and Home Bay), ICE-3G has 1200 m of ice at maximum and the emergence predicted in this region now agrees well with the RSL data. At the northwestern end of the island, the RSL data require a reduction of ice thickness (Milne Inlet, Agu Bay, Brodeur Peninsula, Northern Melville Peninsula, and Igloodik Island). Further to the west, ice is generally thinner (Boothia Peninsula, Bathurst Inlet, Northern Prince of Wales Island and Northern and Southern Somerset Island), and over Banks Island ice is completely absent [*Vincent*, 1983, 1984; *Hodgson and Vincent*, 1984] which also agrees with the DPR maps. To the south of Baffin Island, over Labrador and northeastern Quebec the ice cover is generally thicker (Goose Bay and Hamilton Inlet).

In the southeast region of the Laurentide Ice Sheet, all the RSL data require a substantial thinning of the ice cover coupled with much earlier disintegration of the ice sheet in this area from that specified in ICE-2 (Ottawa, Cornwall, Montreal, Riviere du Loup, and Rimouski). The agreement of ICE-3G predictions to the data is extremely good and has not previously been achieved. The lone exception to this excellent agreement is the Gulf of St. Lawrence site on the north coast. It is, however, surrounded by sites (Moisie, Gaspé, Goose Bay, St. George's Bay and Northwest Newfoundland) which all have good agreement between the ICE-3G predictions and the RSL data, so this site must be considered anomalous. The Newfoundland Ice Cap remains essentially unchanged from ICE-2 with a maximum thickness of

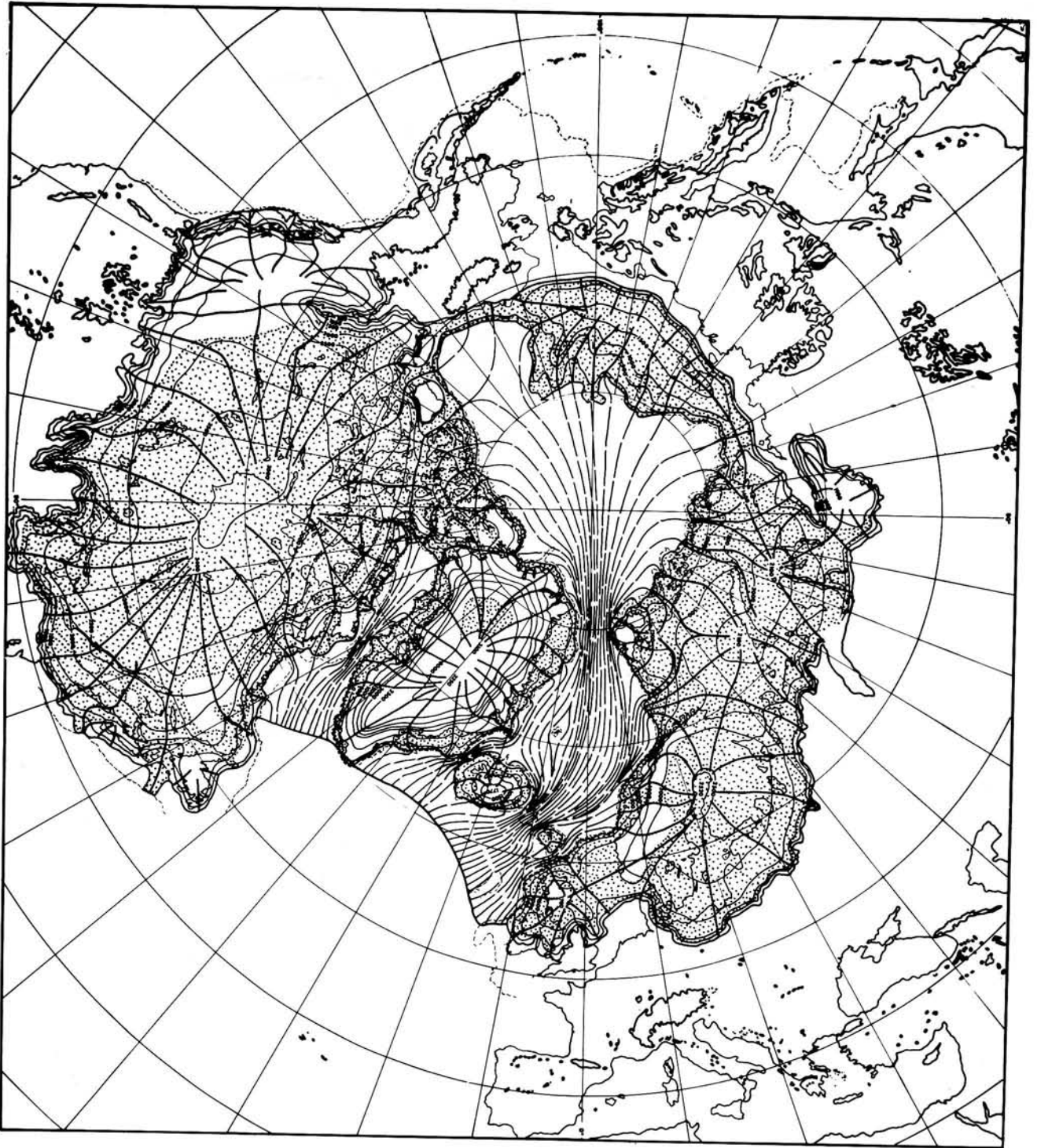


Fig. 8. The DDMX ice cover model at 18 ky BP.
Note the ice cover over the North Sea, Parry Islands,

Baffin Bay, Alaska, Barents Sea, and Asia [from Hughes
et al., 1981].

700 m, which is considerably less than the DDMX value of about 1300 m (St. George's Bay and Northwest Newfoundland). The excellent agreements at St. George's Bay, Moise, Gaspé and Rimouski are obtained by virtually eliminating all ice cover in the Gulf of St. Lawrence. Instead of the 1700 m of ice cover proposed in ICE-2 and the 2000 m in the DDMX model, ICE-3G has only 200 m of ice cover in the Gulf and this ice soon disappears. This early melting agrees with the DPR maps for this area, and the RSL

data from French River and to a lesser extent Tignish and Charlottetown also prefer only a thin veneer of ice.

Further south, from Nova Scotia to Cape Cod the quality of the agreements between ICE-3G predictions and the RSL data vary widely. The agreement at some sites is excellent (Isle of Shoals and Boston), whilst at others it is quite poor (Bay of Fundy, Addison and Plum Island). The sites in this area can all be considered ice-marginal or edge sites and were generally not ice

a

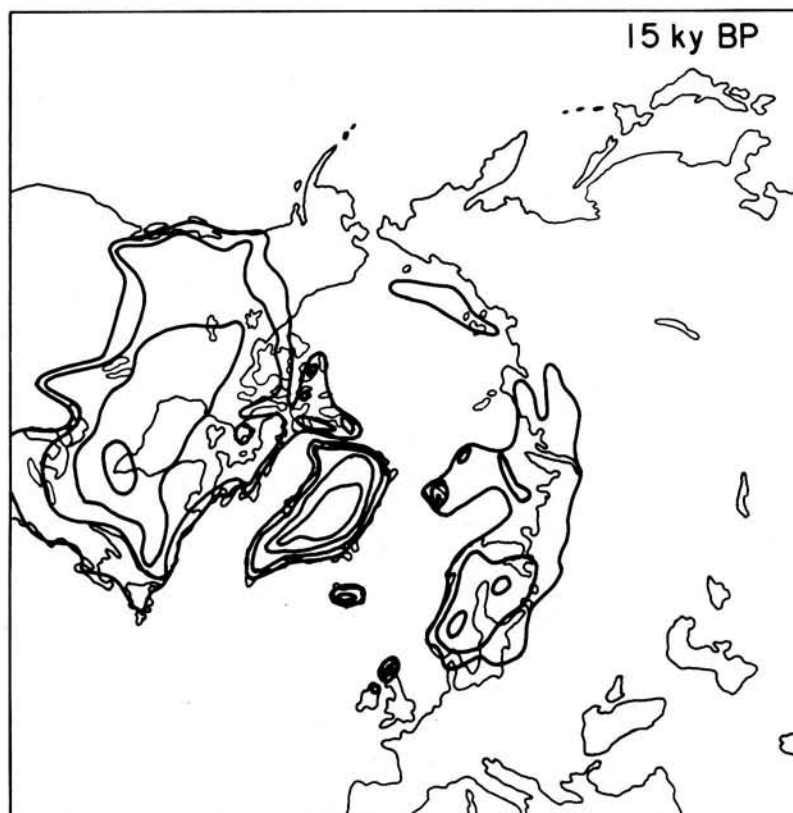
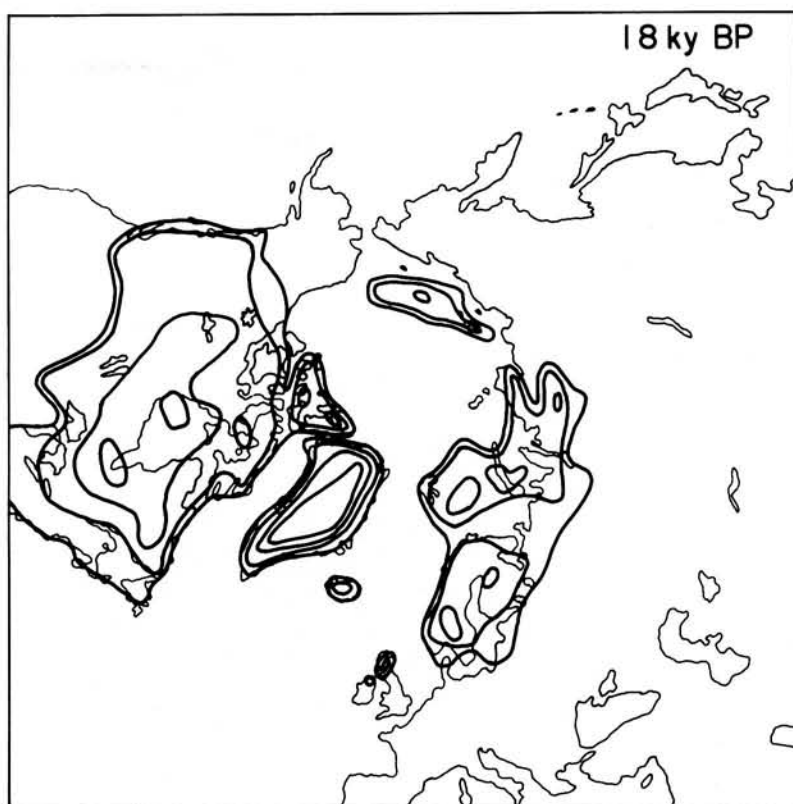


Fig. 9. Northern Hemisphere isopleth maps for ICE-3G. Contour interval is 1 km. Note the rapid deglaciation of the Barents Sea and the separation

of the Laurentide large Cordilleran ice sheets. (b) Northern Hemisphere isopleth maps for ICE-3G.

b

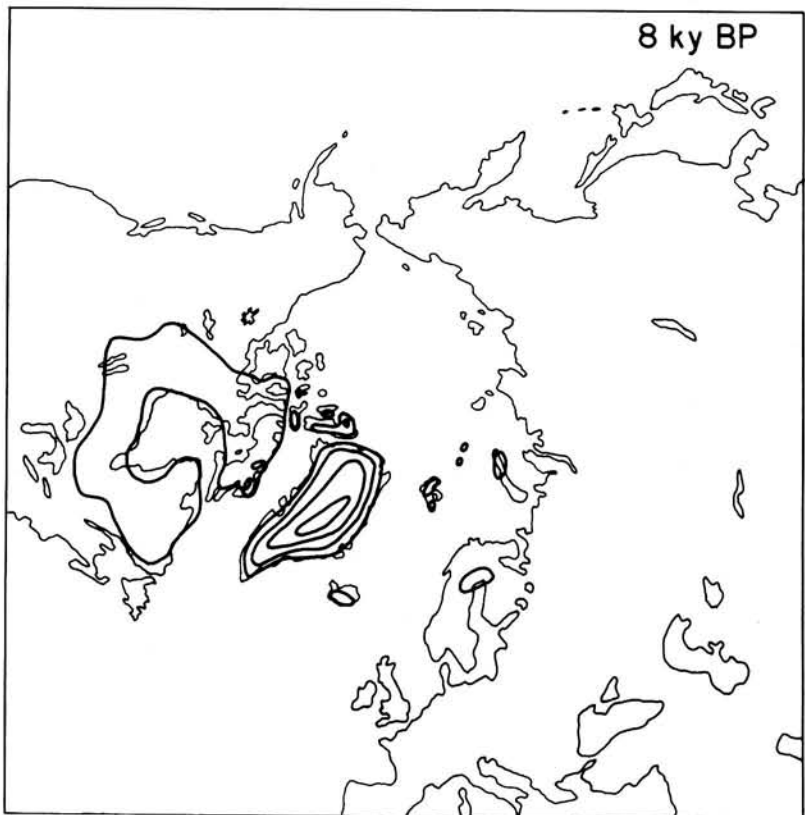
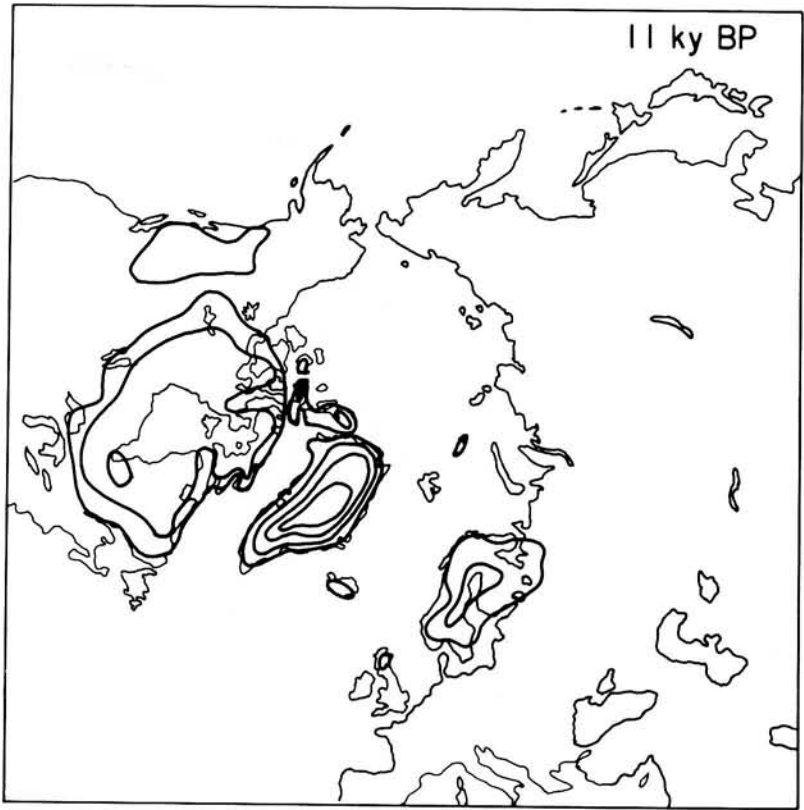


Fig. 9. (continued)

covered during most of the late Pleistocene. The isostatic rebound at an edge site is sensitive to changes in lithospheric thickness, but in ice-covered regions it is much less sensitive [Peltier *et al.*, 1986]. However, even invoking a lithospheric thickness much larger than the 120 km employed, the RSL data at these sites could not all be matched by rebound predictions. Indeed some sites (Addison and Plum Island) could only be fitted if the Earth and ice models were modified so drastically that the rest of the data set could no longer be matched, and therefore such sites must also be considered anomalous. It is most probable that these remaining difficulties will be resolved by employing much higher resolution versions of the deglaciation history.

Returning for a moment to the controversy concerning the number of ice domes comprising the Laurentide Ice Sheet, we find that the ICE-3G model does show high thickness values over James Bay, Keewatin and Foxe Basin (see Figure 9) but these maxima are not nearly so prominent as the polydomal supporters would prefer to see. Whereas during the glaciation of North America, erratic studies [e.g., Shilts *et al.*, 1979; Shilts, 1980; Andrews and Miller, 1979] show grave problems with Flint's monodomal model, the deglaciation model presented here does not discount the possibility of an almost monodomal Laurentide Ice Sheet existing during the earliest part of the last deglaciation phase of the Ice Age.

On the west side of the continent the Cordilleran Ice Sheet (listed in Appendix A as part of the Laurentide Ice Sheet) is essentially unchanged from ICE-2, with the exception of several coastal sites, and it agrees with the DPR maps. Both ICE-2 and ICE-3G have only half the thickness of ice proposed by the DHMX model in this area and there is no ice cover modeled along the south coast of Alaska and the Alaska Peninsula which is evident in the DHMX model. This exclusion of ice cover is required to satisfy the RSL data at Copper River. Unfortunately, there is an absence of RSL data from the Aleutians so that no estimate of ice thicknesses could be made. If an Aleutian Ice Sheet was included it would probably be somewhat larger than the Iceland Ice Sheet but smaller than the East Siberian Sea Ice Sheet and therefore, according to Table 2, it would add between 1 and 2 m to the eustatic sea level rise. The northern Alaska data (Barrow and Nome) appears anomalous as these parts of Alaska were ice-free during the last glaciation [cf. Lea and Waythomas, 1988]. In the Archipelago of southeastern Alaska and northern British Columbia, the ice thickness of ICE-3G is thinner along the coast. The quality of agreement to the data ranges from excellent (Ketchikan and Queen Charlotte Sound) to adequate (Juneau) to poor (Prince Rupert and Queen Charlotte Islands). Over Vancouver Island and southern British Columbia the ice cover is thinner and the southern margin of the ice sheet is repositioned slightly northeastward, which allows for better agreement to the Cordilleran Ice Sheet's southern margin as proposed by Clague *et al.* [1980]. These changes produced excellent agreement at Victoria and quite good agreement at the other sites (North and East Vancouver Island, the Frazer Lowlands and Whatcom) along with better agreement with the DPR maps.

In the High Arctic, the ICE-2 predictions of RSL history were poor due to the very coarse gridding of 5° x 5° and an unsatisfactory distribution of ice. Although the ICE-2 prediction at Bathurst Island is quite good and at Cornwallis Island the predicted emergence is actually too large, when ICE-2 was regridded to a 2° x 2° grid these predictions became much too small. As mentioned at the beginning this section, in order to satisfy these two stations it is necessary to extend the Innuitian Ice Sheet westward over all of the Parry Islands which the DPR maps do not

show. This part of the Innuitian Ice Sheet has a maximum height of nearly 2400 m just to the northwest of Cornwallis Island. To the east over Devon Island, the ice thickness is reduced to a maximum of 1150 m and now the RSL data at Boat Point and Truelove Inlet are matched quite well. Over Ellesmere Island, due to the poor gridding of ICE-2, the ice cover had to be restructured. Generally, the ice cover over Ellesmere Island is thicker, especially in the northernmost part of the island, and the timing of the onset of melting and the melting history are also quite different. These differences allow better fits to the shape of the RSL curves from Cape Storm, South Cape Fiord, Bay Fiord and East Axel Heiberg Island. The thicknesses of ice over southern and central Ellesmere Island are about 1800 and 2800 m, respectively, which are much larger than the maximum 1500 m over southwestern Ellesmere Island that the DHMX model suggests. In northern Ellesmere Island the ice cover is dramatically thicker to a maximum of 2400 m and the northern margin is now north of Ward Hunt Island, which does not agree with the DPR maps. Previously, ICE-2 predicted very small emergence or even submergence at these northern sites, but ICE-3G correctly predicts the observed emergence at most of the sites on northern Ellesmere Island (Archer Fiord, Cape Baird, Discovery Harbour, Alert, Clements Markham Inlet, Disraeli Fiord, Thores River, Rainbow Hill, M'Clintock Inlet and Phillips Inlet). England and associates [England, 1976a, b; 1982, 1983; J. England and J. Bednarski; Post-glacial isobases from northern Ellesmere Island and Greenland: New data, unpublished manuscript, 1985] state that they consider the complex geological evidence to indicate the presence of only a thin ice cover in this area (which formed the evidence upon which the DPR maps were constructed). However, the geological evidence may itself be misleading: if the late Pleistocene ice cover in this region was cold-based (i.e., the basal ice was frozen to the ground) as proposed by Blake [1970] and Hughes and Fastook [1976], erosion would be impossible because there was no ice motion at the interface with the ground and deposition would be impossible because all ice flow lines originate at the ice surface. The ICE-2 model in this area was roughly equivalent to the thin ice cover model suggested by England. To explain the presence of high raised beaches in the area, England suggests that northern Ellesmere Island is undergoing tectonic uplift. Based on numerical experiments involving the inclusion and exclusion of tectonic RSL sites in the Pacific Ocean and general constraints from tectonophysics, we believe it highly probable that any general Ellesmerian tectonic uplift would be slow in comparison to glacial rebound so that clearly, from the RSL computations undertaken at Alert and other sites on northern Ellesmere Island, a thick ice cover is clearly required to accommodate the observed RSL data. This conclusion agrees with the extensive Innuitian Ice Sheet originally proposed by Blake [1970] based on Pumice data collected from the Queen Elizabeth Islands.

Next to be discussed is the Greenland Ice Sheet. Overall the agreement between RSL data and ICE-3G (or ICE-2) predictions are not particularly good for this region. In the far north (Hall Land and Jorgen Bronlund) and the far south (Julianehaab), the ice cover is thicker and, instead of very little emergence or even submergence as suggested by ICE-2, ICE-3G now predicts the observed emergence adequately. In central Greenland, the ice cover has been thickened from a maximum of 3500 m to 3850 m, which is considerably larger than the value of 3250 m proposed by the DHMX model. Unfortunately, the increase in overall ice thickness only slightly improves the fits. Most sites in central Greenland have RSL data which indicate very sharp and very steep emergence over time (Sondre Stomfjord, Skeldal, and Mesters

Vig). Since the steep sea level curves are not correctly predicted by ICE-3G no matter how the ice model is adjusted, they may indicate the presence of local or regional lithospheric anomalies. Clark's [1976] hypothesis that the inclusion of the gravitational effect of the massive ice sheets would allow correct prediction of these very rapid emergence curves appears then to be completely incorrect. Tectonic uplift may be one possible explanation for these curves; another may be changes in local or regional Earth rheology. Most likely, however, is the suggestion that follows from the recognition that all of these sites are in deeply fiorded terrain so that rapid retreat of ice up the fiords and rebound of the crust with a significant elastic component could explain the very steep RSL curves (similar examples are found in Norway as we shall see).

The Deglaciation of Europe and Asia

The ice sheets of Europe are smaller in extent and thickness than their North American counterparts, and in Asia the very existence of any extensive ice cover is still widely debated. Climatological considerations may imply that the large Asian landmass inhibited the growth of large ice sheets [North *et al.*, 1981]. In ICE-3G the ice cover for Europe and Asia consists of the Fennoscandian, Barents Sea and Kara Sea Ice Sheets (which combine to form the Northern European Ice Sheet Complex), the separate East Siberian Sea Ice Sheet, and ice caps on Iceland and Scotland. The deglaciation history for these ice sheets is summarized in Figure 9. The Fennoscandian Ice Sheet has been constructed with its central dome located over the northern end of the Gulf of Bothnia as implied by the observed free-air gravity anomaly. The location of the ice dome agrees with that suggested by ICE-2, the DHMX model, and Grosswald [1980], but the central thickness of the dome is now only 2200 m. This value is smaller than the 2500 m of ICE-2 and the DHMX model and the 3000 m of Grosswald's model (subsequently referred to as the G80 model), but the use of this smaller value allows excellent agreement with the RSL data in this area (Stockholm, Angermanland and Kristiinankaupunki). In addition, the southern margin of the Fennoscandian Ice Sheet is much further north than in the other models. Whereas the other models have the southern margin well south of the Baltic Sea and the Gulf of Finland, ICE-3G's margin has southernmost Sweden and the southern Baltic Sea unglaciated and the margin only just south of the Gulf of Finland. The excellent agreement with the wealth of RSL data in these areas allows confidence in the above conclusions (Frederikshavn, Korsor, Rodbyhavn, Goteborg, Onsala, East Blekinge, Helsinki, Tallinn, and Sarema). Geological evidence available in this area, especially in the Gulf of Finland, is commonly insufficient to confidently infer ice marginal positions [Andersen, 1981a], so glacial isostatic modeling allows an estimate where none was available previously. Both ICE-2 and ICE-3G place the western margin along the Norwegian coast, which contradicts the DHMX and the G80 models since they both have the North Sea covered with over 1000 meters of ice. The RSL data from southern Norway (Skuloy, Stette, Sula, Leinoy, Fønnes, and Lista) can be matched by ICE-3G predictions, but cannot possibly be matched by any model in which the North Sea is ice covered. As we shall see later, the RSL data from Great Britain also repudiate the suggestion of an ice-covered North Sea. This conclusion further agrees with evidence from the Shetland Islands collected by Hoppe [1974] and the lack of isostatic rebound in the North Sea as calculated by Milling [1975] and Holmes [1977]. Along the central Norwegian coast the ICE-3G model predicts

RSL histories which agree very well with the RSL data (Verdalsora, Frosta, Bjugn, Froya, and Hitra). These excellent fits do not generally extend past 10,000 years B.P. as the data show a very sharp decrease in relative sea level from 11,000 to 10,000 years B.P. It is not known what causes these sharply varying RSL curves which are somewhat reminiscent of those previously discussed from Greenland. The following section will discuss these curves in more detail.

The northern and eastern margins of the Fennoscandian Ice Sheet merge into the Barents Sea and Kara Sea Ice Sheets respectively. Although an extensive ice sheet in the Spitsbergen area was envisaged at the turn of the century [De Geer, 1900], the total coverage of the Barents Sea with a large ice sheet was not seriously proposed until the early 1960s [Corbel, 1960; Grosswald, 1963; Schytt *et al.*, 1968] based on work undertaken on Spitsbergen by Büdel [1960], Feyling-Hansen and Olsson [1960], Blake [1961], and Olsson and Blake [1962]. The estimates for both extent and thickness of the Barents Sea Ice Sheet were derived from systematic studies of isostatic land rise. Schytt *et al.* [1968] extended this data base by studying raised beaches over the entire Spitsbergen area. They found two levels on these beaches that were particularly easy to identify due to an abundance of pumice, which also allowed the age of the upper level to be estimated to be 6500 radiocarbon years B.P. From their pumice data, they constructed an isobase map for the Barents Sea (shown in Figure 10) which indicated that the center of uplift was near the center of the Barents Sea, which is strong evidence in support of a large Barents Sea Ice Sheet. (These pumice data were added directly to the existing RSL data at each of the 12 Spitsbergen sites, but not at the two Franz Joseph Land sites as the control was considered to be inadequate in that area). A large $\delta^{18}\text{O}$ meltwater spike determined from a deep-sea core (PS21295-4) taken from Fram Strait, located just to the west of Spitsbergen, also implies the presence of a large Barents Sea Ice Sheet [Jones and Keigwin, 1988]. Further geological evidence comes from the study of striations and erratics on Hopen Island [Hoppe *et al.*, 1969] which indicate a westerly flow of ice from the Barents Sea towards Spitsbergen (which cannot be caused by a local ice sheet on Spitsbergen), and seismological investigations undertaken by Sundvor [1974] determined that the Quaternary sediments on the Barents Sea floor may indicate a more widespread ice sheet than previously suggested. Geophysical evidence such as polar wandering also appears to require a large Barents Sea Ice Sheet [Peltier, 1988b]. It was this latter evidence which in fact first initiated our inclusion of this ice sheet in ICE-3G.

Our Barents Sea Ice Sheet was constructed from ice margin isochrones compiled by Andersen [1981b] and has a central thickness of 2200 m. This value is between the 2100 m suggested by the DHMX model and the 2500 m suggested by the G80 model. Due to marine-base ice sheet instability outlined by Stuiver *et al.* [1981], the Barents Sea Ice Sheet is expected to disintegrate rapidly as global sea level rises, so that by 14,000 years B.P. (S.J. Lehman, personal communication, 1988) only ice caps on Spitsbergen, Franz Joseph Land and Novaya Zemlya remain. This early deglaciation is also evident from oxygen-isotope data collected from Fram Strait off the west coast of Spitsbergen, which shows a significant increase in ^{16}O around 15 kyr B.P. presumably due to rapid melting of the Barents Sea Ice Sheet [Jones and Keigwin, 1988]. Forman *et al.* [1987] suggested that the early and rapid deglaciation of the Barents Sea Ice Sheet followed by slower deglaciation of the remnant ice caps caused the observed sharp RSL curves seen at many of the western Spitsbergen sites (Hornsund, Kapp Linne, Billefjorden, Prins Karls Forland, and

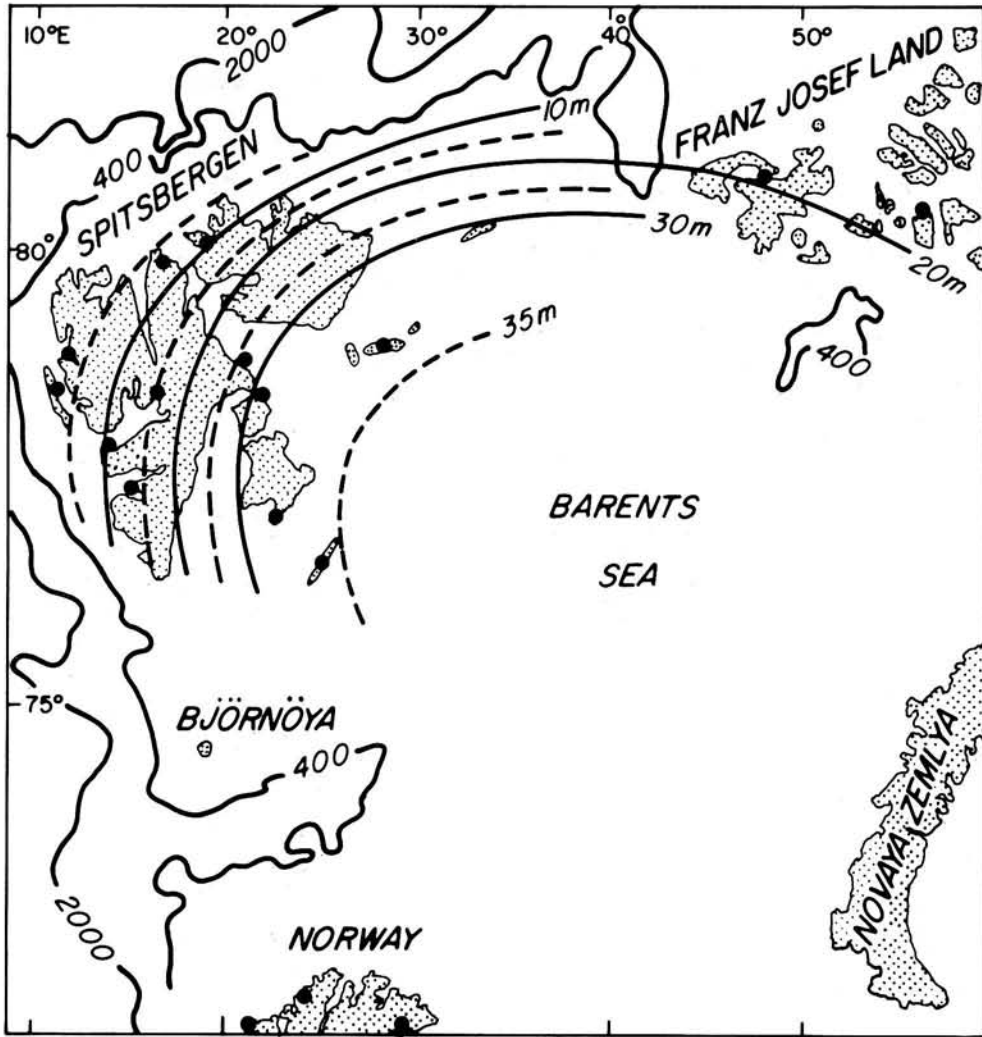


Fig. 10. Barents Sea isobase map based on a pumice line from a volcanic event dated 6500 years B.P. [from Schytt *et al.*, 1968].

Broggerhalvoya). These sharp RSL curves are predicted by ICE-3G particularly well, especially at Prins Karls Forland. The old ICE-2 model did not have a Barents Sea Ice Sheet and instead had only ice caps on Spitsbergen, Franz Joseph Land and Novaya Zemlya, and thus its predictions in this region are very poor. The northernmost Fennoscandian RSL data are either insensitive to the presence of a Barents Sea Ice Sheet (Kola Bay and Varanger Fjord) or only slightly prefer the inclusion of the ice sheet (Kvalvika and And Fjord), but there is a definitely strong preference with the Spitsbergen RSL data. At the five southeastern sites on Spitsbergen located closest to the center of the ice sheet (Wilhelmoya, Barentsoya, Edgeoya, Kong Karl Land, and Hopen Island), the rebound predictions of ICE-3G agree very well with the RSL data but ICE-2 (without any Barents Sea Ice Sheet) dramatically underestimates the amount of uplift. On the north coast of Spitsbergen and on Franz Joseph Land, ICE-3G predictions are preferred (Sorgfjorden, Murchisonfjorden, Zemlya George, and Ostrov M'Clintock), but only after moving the northern margin further to the north than suggested by Andersen [1981b] or modeled by ICE-2.

To the east of Novaya Zemlya ICE-2 had only a small ice cap on the Yamal Peninsula, but ICE-3G includes the Kara Sea and the East Siberian Sea Ice Sheets. The former ice sheet is formed from

the Kara Sea Ice Dome and the Putorana Plateau Glacier Complex as proposed by the G80 model, with central thicknesses of 2400 and 2300 m respectively. These values are larger than those suggested by the DHMX model of 2100 and 2000 m, respectively. The predominant geological evidence which aided in the construction of the G80 model in this area comes in the form of lacustrine deposits from proglacial lakes and meltwater drainage along the southern margin [e.g., Volkov *et al.*, 1978]. The East Siberian Sea Ice Sheet is based on circumstantial evidence compiled by Denton and Hughes [1981] and has a central thickness of 2000 m. Although no RSL data are available for these areas (except for the lone site of Yana River, Siberia, which is adequately predicted by both ice models) the inclusion of these two ice sheets increases the maximum sea level rise by 10 m (refer to Table 2) thereby allowing better agreement with the $\delta^{18}O$ data.

The last two components of the Northern Hemisphere ice cover are the ice caps on Iceland and Scotland. The value of the maximum thickness of the Iceland Ice Cap is 1900 m which is larger than the ICE-2 value of 1500 m and the DHMX value of 1800 m, but melting now begins 2000 years earlier than in the ICE-2 model. The margins at the last glacial maximum roughly follow those inferred from end-moraine studies [e.g., Einarsson, 1973]. The agreement between the predicted sea level histories of

ICE-3G to the RSL data for the Iceland sites (Stadarholskirkja, Akranes, and Reykjavik) are excellent and the improvements from the predictions of ICE-2 dramatic.

Over Scotland ICE-3G, the G80 model, and the DHMX model suggest a maximum thickness of 1700, 1700 and 1800 m respectively, but ICE-2 had a thickness of only 1000 m. However, ICE-3G proposes a much more restricted ice cap in area than do the other models. In the G80 and DHMX models land as far south as southern Wales is ice covered and the ice cap is connected to the Fennoscandian Ice Sheet by an ice-covered North Sea; although ICE-2 does not have the latter feature it does have ice extending south into northern Wales. These models are not supported by the RSL data. ICE-3G, however, only has ice covering Scotland, north of the Southern Uplands, and Northern Ireland. At sites located along ICE-3G's southern margin, which are well within the margins of the other models, ICE-3G correctly predicts the somewhat stable relative sea level implied by the data whereas the other models predict strong emergence of the land (Firth of Forth, Port Glasgow, Ayr, the Machars, and Belfast). Further south the predictions of ICE-3G agree with the observed submergence while the other models still predict strong emergence (Tees River, Cumberland, and Merseyside). The hypothesis of an ice-covered North Sea during the last 18,000 years is completely rejected by the RSL data from both Great Britain and southern Norway and geological evidence from Shetland [Hoppe, 1974] and the North Sea floor (Holmes 1977).

The Deglaciation of Antarctica

The ice sheet on Antarctica can be divided into the East and West Antarctic Ice Sheets separated by the Transantarctic Mountains. Although it is grounded over several subglacial basins, the base of the East Antarctic Ice Sheet is largely terrestrial since most of the subglacial basins would be above sea level if the ice sheet were removed and isostatic rebound of the bed was complete [Benley, 1972; Drewry, 1983]. Several geological studies imply that this ice sheet was relatively stable during the last deglaciation event [Mercer, 1968; Denton *et al.*, 1971; Stuiver *et al.*, 1981]. The West Antarctic Ice Sheet overlies a generally rugged bedrock floor, much of which is now well below sea level and would remain so if the ice sheet were removed and the floor allowed to adjust isostatically [Drewry, 1983]. The West Antarctic Ice Sheet was and remains a marine-based ice sheet [Mercer, 1968] and thus became unstable as sea level rose (as described by Stuiver *et al.* [1981]).

In ICE-2, only the melting component of the Antarctic Ice Sheet was included in the compilation of Wu and Peltier [1983] but here, even though it does not effect the sea level calculation, the total ice sheet thickness is presented so that all ice sheets are presented in the same format. The melting component of ICE-3G has been modified so that the Antarctic Ice Sheet now begins to deglaciate when the ice sheets of the Northern Hemisphere are at their maximum rates of deglaciation as discussed by Peltier [1988a]. In the ICE-3G model developed herein the Antarctic Ice Sheet starts to deglaciate at 9000 years B.P. so as to allow better agreement with the far-field ocean site of Wairau Valley, New Zealand. This site was selected to control the timing of Antarctic deglaciation because it has one of the best defined far-field RSL histories. The new melting component is added to the present Antarctic ice cover, based on reconstructions by Drewry [1982], Drewry *et al.* [1982], and Hughes *et al.* [1981, 1985]. The estimate of the maximum thickness of ice present during the last glaciation is limited by the elevation of nunataks [e.g., Craddock *et al.*,

1964]. Figure 11 summarizes the melting history of the Southern Hemisphere, and Appendix B presents RSL estimates for sites in ice-covered regions of the Southern Hemisphere plus the Wairau Valley site. Unfortunately, RSL data for Antarctica is scarce and data for only four sites are available. In fact any type of data which aids in establishing chronological control of the Antarctic Ice Sheet is scarce, but there may be some promise from the study of sedimentation rates beneath Antarctic ice shelves (J. Westgate, personal communication, 1989). Although for most of Antarctica the total ice thickness changes are the same for both ice models, ice grid elements in the immediate vicinity of these four sites are adjusted in order to obtain better agreement between predictions and observations. The fits to the data range from good (Olaf Land and Knox Coast) to adequate (Palmer Peninsula) to poor (McMurdo Sound). The melting component of the Antarctic Ice Sheet is responsible for 26 m of the total 115 m of sea level rise predicted in the western Pacific Ocean. If the present Antarctic Ice Sheet were to melt completely, the sea level would rise 69 m with an additional 7-m rise if the Greenland Ice Sheet also melted (refer to Table 2).

The only other ice sheet in the Southern Hemisphere large enough to warrant being modeled was the Patagonian Ice Sheet. This ice sheet, modeled after the DHMX model which followed the arguments for a restricted ice sheet of Polanski [1965], consists of a glacial complex along the Chilean coast south of 40°S with a maximum ice thickness of just over 400 m. Initially it was thought that the timing of melting for the Patagonian Ice Sheet would mimic that of the Antarctic Ice Sheet, but the RSL data in this area implied that this could not have occurred. In ICE-3G the Patagonian Ice Sheet disappears completely by 14,000 years B.P. (as suggested by Rodbell and Birkland [1988] on geological evidence), which allows for fairly good agreement between predicted and observed sea level at the Patagonian sites of Bahia Gente Grande and Puerto del Hambre. The earlier removal of the Patagonian Ice Sheet also concurs with pollen evidence from Tierra del Fuego [Markgraf, 1987] and in fact RSL data from the Beagle Channel and La Mision actually show a preference for the RSL estimates based on the ICE-2 model, which has no Patagonian Ice Sheet.

CONCLUSIONS

Prior to the present work, glacial isostatic rebound modeling has been used primarily to investigate the rheology of the Earth's interior, in particular the viscosity profile of the mantle [Peltier and Andrews, 1976; Wu and Peltier, 1983]. Both of these previous analyses employed a priori reconstructions of late Pleistocene ice loads and focused on the effect on the RSL predictions of varying the parameters that control the radial viscoelastic structure of the Earth's interior. From this focused modeling exercise a variety of other geophysical observations could be predicted and compared to the observations. Although the ice loads employed in these earlier works were fairly realistic, the finer details were absent. In the present work a single "standard" model of the Earth's interior was selected, based on the simultaneous agreement of the free-air gravity anomalies over Laurentide and Fennoscandia, the observed nontidal acceleration of the Earth, and relative sea level data from Canada and along the United States east coast [Peltier *et al.*, 1986]. The finite grid elements of the ice load were refined from the previous 5° x 5° resolution to an approximate 2° x 2° resolution and the ocean grid was also refined so as to have better resolution along the coasts [Peltier, 1988a]. Using an iterative process the thicknesses of ice on the finite ice grid elements were

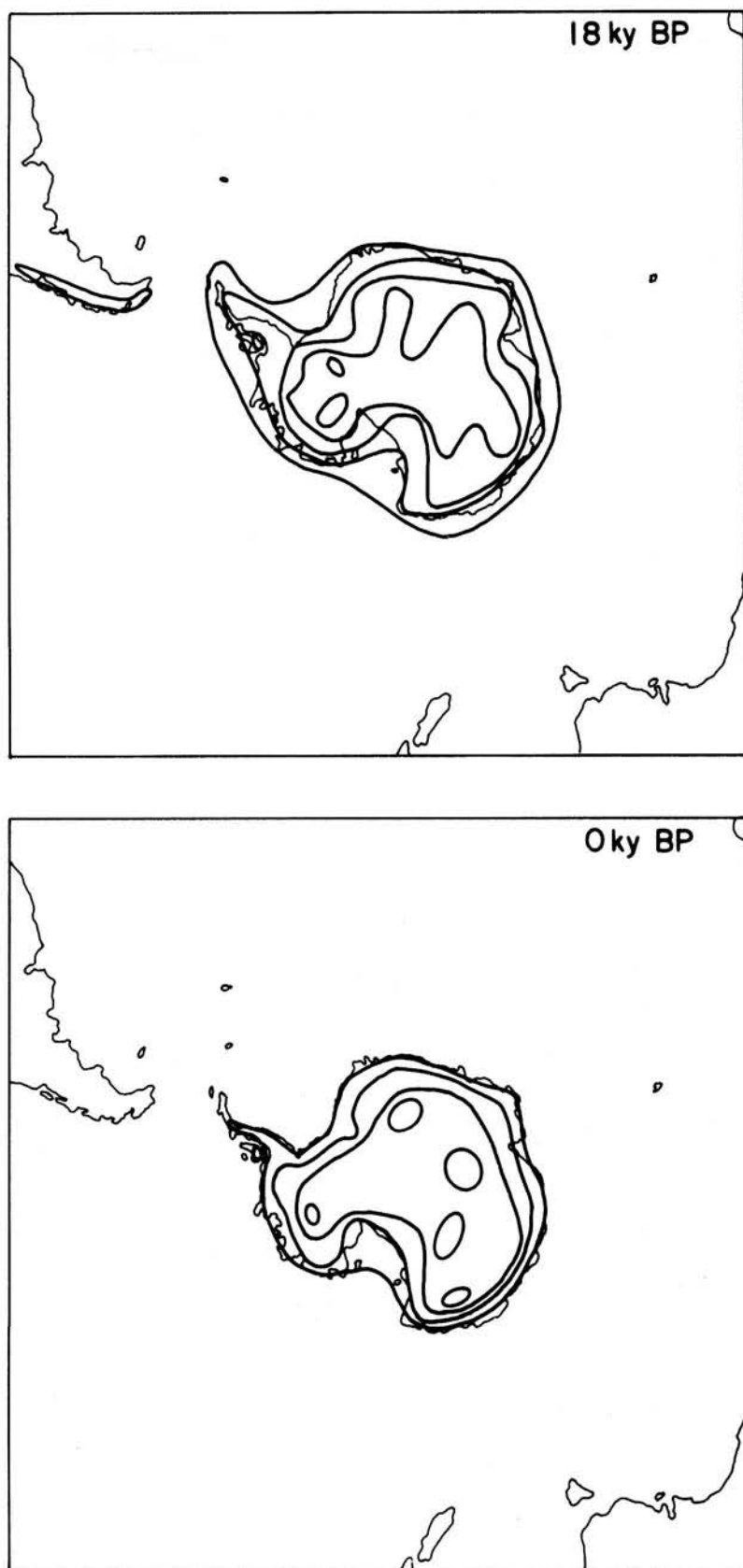


Fig. 11. Southern Hemisphere isopleth maps for ICE-3G. Contour interval is 1 km. Note the large changes to the West Antarctic Ice Sheet.

varied and the results of the computations were compared to a vastly expanded RSL data base. This study made use of 192 sites at which RSL data has been collected whereas in the previous work of Wu and Peltier [1983] only 45 sites were employed as control. The new model of deglaciation, ICE-3G, is able to fit all the available RSL data to within the minimum variance whereas the precursor model ICE-2 was only able to fit to within twice the minimum variance. Those regions where good agreements are difficult or even impossible to obtain using the existing isostatic rebound modeling process may give future researchers an indication as to where further field work or computer modeling are required. Regions from which RSL data is largely absent, such as the Parry Islands, Siberia and Antarctica, should also be investigated further.

The relative uniqueness of the ICE-3G model has hopefully been established, at least circumstantially, by the large number of RSL histories to which the predicted responses have been favorably compared. Since the predicted responses are most

sensitive to local changes in ice thickness, each RSL site allows a reasonably accurate estimate of local ice thickness; however, this is only possible if the timing of local deglaciation is known. To establish the chronology of deglaciation, geological retreat maps (based on terminal moraines and other geological evidence) were examined and incorporated into the model. There is of course uncertainty in regions which have little RSL data or limited geological evidence (such as most of Siberia). Because $\delta^{18}O$ data allow an estimate of the total ice volume, by subtracting the volume estimates for the better-defined ice sheets one may estimate the volumes of the missing or poorly defined ice sheets. This process cannot however delineate the extent or thickness of these ice sheets independently. For ICE-3G this means that the Kara Sea and East Siberian Sea Ice Sheets are only crude estimates and may be quite different in reality from those modeled here. The remaining ice sheets are well constrained by RSL, geophysical or geological data.

The overall conclusion for ice cover in the Northern Hemisphere, based on the construction of ICE-3G, is that ice has been redistributed northward from all previous models. For example, the Laurentide and Fennoscandian Ice Sheets are slightly thinner here than in previous estimates whilst the Innuitian and Barents Sea Ice Sheets are thicker and more extensive. In the Southern Hemisphere, far-field ocean RSL data from Wairau Valley, New Zealand allow us to infer [after Peltier, 1988a] that the Antarctic component of melting was initiated up to 9000 years after the Northern Hemisphere component. Figure 12a summarizes the melting histories of the various ice masses in terms of their contribution to the total sea level rise predicted off the Huon Peninsula, Papua New Guinea. The delayed melting of the Antarctic Ice Sheet is clearly evident as is the relatively slow deglaciation of the North American ice sheets and the rapid deglaciation of the mostly marine-based European ice sheets. In Figure 12b we compare the global eustatic sea level curve for the ICE-3G model to individual RSL histories in the Western Pacific and the Caribbean. These comparisons demonstrate the extent to which, even at sites which are remote from the main centers of deglaciation, individual sea level histories may deviate from eustatic. In a future paper a further 200 sites for which RSL data have been compiled will be employed to verify the consistency the ICE-3G model of deglaciation and to assess the sensitivity of its predictions to changes in Earth structure [A. M. Tushingham and W. R. Peltier, submitted manuscript, 1990].

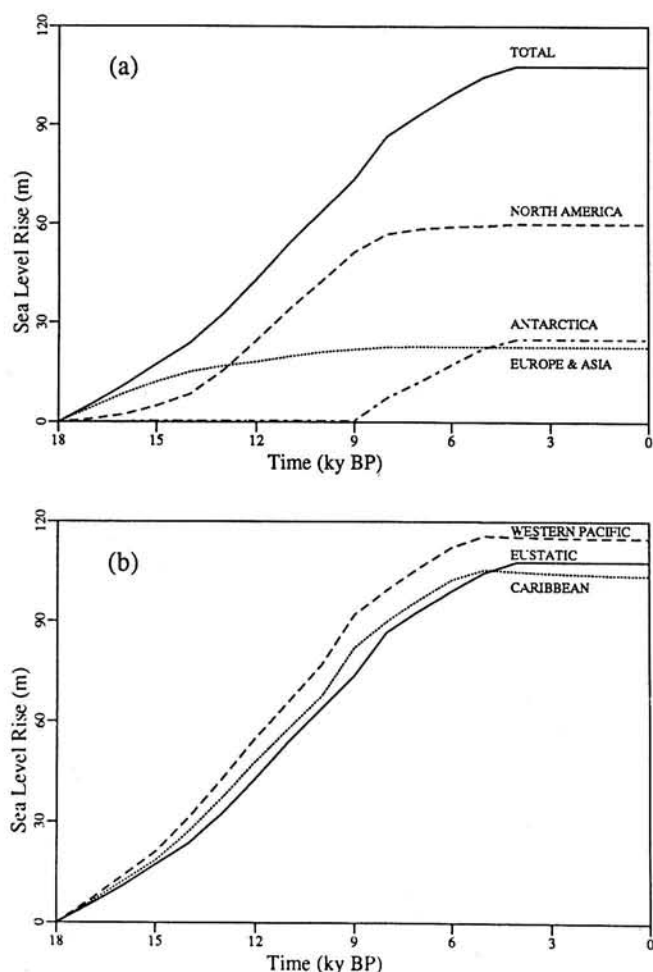


Fig. 12. (a) The "eustatic" sea level rise due to various ice masses. The solid curve represents the total of all ice sheets, the dashed curve represents the North American ice sheets (Laurentide, Innuitian, and Greenland), the dotted curve represents the European and Asian ice sheets (Fennoscandian, Barents Sea, Kara Sea, East Siberian Sea, Iceland and Scotland), and the dash-dotted curve represents the Antarctic and Patagonian Ice Sheets. (b) The difference between eustatic and local sea level rises. The solid curve represents the eustatic rise, the dashed curve represents the rise at the location of core V28-238, and the dotted curve represents the rise at Barbados. Note the raised beaches (circa 6 kyr B.P.) on the two local sea level curves.

Appendix A: Tabulation of the ICE-3G model of late Pleistocene deglaciation. To be available on microfiche only. Appendix B: Comparison of relative sea level predictions for the new deglaciation model ICE-3G and the old deglaciation model ICE-2 along with observations for all ice covered sites. To be available on microfiche only.

REFERENCES

- Andersen, B. G., Late Weichselian ice sheets in Eurasia and Greenland, *The Last Great Ice Sheets*, pp. 3-66, G. H. Denton and T. J. Hughes eds., John Wiley and Sons, Inc., New York, 1981a.
- Andersen, B. G., Schematic Weichselian ice-sheet margins in the Barents Sea area, *The Last Great Ice Sheets*, map 1.3, G. H. Denton and T. J. Hughes eds., Wiley and Sons, Inc., New York, 1981b.
- Andrews, J. T. and G. H. Miller, Glacial erosion and ice sheet divides, northeastern Laurentide Ice Sheet, on the basis of the distribution of limestone erratics, *Geology*, 7, 592-596, 1979.
- Andrews, J. T., G. H. Miller, J.-S. Vincent, and W. W. Shilts, Quaternary correlations in Arctic Canada, *Geol. Surv. Can. Pap.*, 84-10, pp. 127-134, 1984.

- Bard, E., B. Hamelin, R. G. Fairbanks, and A. Zindler, Calibration of ^{14}C over the last 80,000 years using U/Th ages obtained by mass spectrometry on Barbados coral, *Nature*, 345, 405-410, 1990.
- Bentley, C. R., Subglacial rock surface topography, *Antarctic Map Folio ser.*, plate 7, folio 16, Am. Geogr. Soc., New York, 1972.
- Berger, W. H. and J. S. Killingley, Glacial Holocene transitions in deep-sea carbonates: selective dissolution and the stable isotope signal, *Science*, 197, 563-566, 1977.
- Berger, W. H., R. F. Johnson, and J. S. Killingley, 'Unmixing' of the deep-sea record and the deglacial meltwater spike, *Nature*, 269, 661-663, 1977.
- Blake, W., Jr., Radiocarbon dating of raised beaches in Nordaustlandet, Spitsbergen, *Geol. Arctic*, 1, 133-145, 1961.
- Blake, W., Jr., Studies of glacial history in Arctic Canada, I, Pumice, radiocarbon dates and differential postglacial uplift in the eastern Queen Elizabeth Islands, *Can. J. Earth Sci.*, 7, 634-664, 1970.
- Blake, W., Jr., Sea and land relations during the last 15,000 years in the Queen Elizabeth Islands, Arctic Archipelago, *Geol. Surv. Can. Pap.* 76-1B, 201-207, 1976.
- Bowen, D. Q., *Quaternary Geology*, 221 pp., Pergamon, New York, 1978.
- Broecker, W. S. and J. Van Donk, Insolation changes, ice volumes, and the ^{18}O record in deep sea cores, *Rev. Geophys.*, 8, 169-198, 1970.
- Broecker, W. S., D. L. Thurber, J. Goddard, T.-H. Ku, R. K. Matthews, R. K. and K. J. Mesolella, Milankovitch hypothesis supported by precise dating of coral reefs and deep-sea sediments, *Science*, 159, 297-300, 1968.
- Büdel, J., Die Frostschutt-Zone Südost-Spitsbergens. In *Colloquium Geographicum*, 6, pp. 105, 1960.
- Chappell, J., A revised sea-level record for the last 300,000 years from Papua New Guinea, *Search*, 14, 99-101, 1983.
- Chappell, J., and N. J. Shackleton, Oxygen isotopes and sea level, *Nature*, 324, 137-140, 1986.
- Clague, J. J., J. E. Armstrong, and W. H. Mathews, Advance of Late Wisconsin Cordilleran Ice Sheet in southern British Columbia since 22,000 yr B.P., *Quat. Res.*, 13, 322-326, 1980.
- Clark, J. A., Greenland's rapid postglacial emergence: A result of ice-water gravitational attraction, *Geology*, 4, 310-312, 1976.
- Clark, J. A., W. E. Farrell, and W. R. Peltier, Global changes in postglacial sea level: A numerical calculation, *Quat. Res.*, 9, 265-287, 1978.
- Corbel, J., Le soulèvement des terres autour de la mer de Barentz, *Rev. Geogr. Lyon*, 35, 253-274, 1960.
- Craddock, C., J. J. Anderson and G. F. Webers, Geologic outline of the Ellsworth Mountains, *Antarctic Geology*, pp. 155-170, J. R. Aide ed., North-Holland Publishing Company, Amsterdam, 1964.
- De Geer, G., Om östra Spetsbergens glaciation under istiden, *Geol. Fören. Förh.* 22, 427-436, 1900.
- Denton, G. H. and T. Hughes, *The Last Great Ice Sheet*, 484 pp., John Wiley and Sons, Inc., New York, 1981.
- Denton, G. H., R. L. Armstrong and M. Stuiver, Late Cenozoic glacial history of Antarctica, *Late Cenozoic Glacial Ages*, pp. 267-306, K.K. Tirekian ed., Yale University Press, New Haven, 1971.
- Drewry, D. J., Ice flow, bedrock, and geothermal studies from radio-echo sounding inland of McMurdo Sound, Antarctica, *Antarctic Geoscience*, pp. 977-983, C. Craddock, ed., University of Wisconsin Press, Madison, 1982.
- Drewry, D. J., Antarctica: Glaciological and geophysical folio, Scott Polar Res. Inst., Univ. of Cambridge, 1983.
- Drewry, D. J., S. R. Jordan and E. Jankowski, Measured properties of the Antarctic Ice Sheet: Surface configuration, ice thickness, volume, and bedrock characteristics, *Ann. Glaciol.* 3, 83-91, 1982.
- Dyke, A. S., and V. K. Prest, Late Wisconsin and Holocene retreat of the Laurentide Ice Sheet, map 1702A, *Geol. Surv. Can.*, 1987a.
- Dyke, A. S., and V. K. Prest, Paleogeography of North America, 18,000 - 5,000 years ago, map 1703A, *Geol. Surv. Can.*, 1987b.
- Dyke, A. S., L. A. Dredge, and J.-S. Vincent, Configuration and dynamics of the Laurentide ice sheet during the late Wisconsin maximum, *Geogr. Phys. Quat.*, 36, 5-14, 1982.
- Dziewonski, A. M. and D. L. Anderson, Preliminary reference Earth model, *Phys. Earth. Planet. Inter.*, 25, 279-356, 1981.
- Einarsson, T., Geology of Iceland, *Arctic Geol. Mem.*, 19, 171-175, 1973.
- Emiliani, C., Depth habitats of some species of pelagic foraminifera as indicated by oxygen isotope ratios, *Am. J. Sci.*, 252, 149-158, 1954.
- Emiliani, C., Pleistocene temperatures, *J. Geol.*, 63, 538-578, 1955.
- England, J., Post-glacial isobases and uplift curves from the Canadian and Greenland high arctic, *Arctic Alpine Res.*, 8, 61-78, 1976a.
- England, J., Late Quaternary glaciation of the eastern Queen Elizabeth Island, N.W.T., Canada: Alternative models, *Quat. Res.*, 6, 185-202, 1976b.
- England, J., Post-glacial emergence along northern Nares Strait, *Geoscience*, 8, 65-75, 1982.
- England, J., Isostatic adjustments in a full glacial sea, *Can. J. Earth Sci.*, 20, 895-917, 1983.
- Epstein, S., R. Buchsbaum, J. A. Lowenstam, and H. C. Urey, Carbonate-water isotopic temperature scale, *Geol. Soc. Am. Bull.*, 62, 417-426, 1951.
- Fairbanks, R. G., A 17,000-year glacio-eustatic sea level record: Influence of glacial melting rates on the Younger Dryas event and deep-ocean circulation, *Nature*, 342, 637-641, 1989.
- Farrell, W. E., and J. A. Clark, On post-glacial sea level, *Geophys. J. R. Astron. Soc.*, 46, 647-667, 1976.
- Feyling-Hansen, R. W. and I. U. Olsson, Five radiocarbon datings of post Glacial shorelines in Central Spitsbergen, *Norsk Geogr. Tidsskr.*, 17, 122-131, 1960.
- Flint, R. F., Growth of the North American ice sheet during the Wisconsin age, *Geol. Soc. Am. Bull.*, 54, 325-362, 1943.
- Flint, R. F., *Glacial Geology and the Pleistocene Epoch*. 589 pp., John Wiley, New York, 1949.
- Forman, S. L., D. H. Mann, and G. H. Miller, Late Weichselian and Holocene relative sea level history of Bröggerhalvöya, Spitsbergen, *Quat. Res.*, 27, 41-50, 1987.
- Gilbert, F., and A. M. Dziewonski, An application of normal mode theory to retrieval of structural parameters and source mechanisms from seismic spectra, *Philos. Trans. R. Soc. London Ser. A.*, 278, 187-269, 1975.
- Grosswald, M. G., The raised shore-lines of the Franz Joseph Land and the late Quaternary history of the archipelago ice sheets, in *Glaciological Researches Articles, IX Section of IGY Program*, Vol. 9, Academy of Science, USSR, 1963.
- Grosswald, M. G., Late Weichselian ice sheet of northern Eurasia, *Quat. Res.*, 13, 1-32, 1980.
- Hall, D. H., A seismic isostatic analysis of crustal data from Hudson Bay, *Geol. Surv. Can. Pap.*, 68-53, 337-364, 1969.
- Haskell, N. A., The motion of a viscous fluid under a surface load, I, *Physics*, 6, 265, 1935.
- Hays, J. D., J. Imbrie, and N. J. Shackleton, Variations in Earth's orbit: Pacemaker of the ice ages, *Science*, 194, 1121-1132, 1976.
- Hodgson, D. A. and J.-S. Vincent, A 10,000 yr B.P. extensive ice shelf over Viscount Melville Sound, Arctic Canada, *Quat. Res.*, 22, 18-30, 1984.
- Holmes, R., Quaternary deposits of the central North Sea, 5. The Quaternary geology of the U.K. sector of the North Sea between 56° and 58°N, *Rep. Inst. Geol. Sci.* 77/14, 50 pp., London, 1977.
- Hoppe, G., The glacial history of the Shetland Islands, *Inst. Br. Geogr. Spec. Publ.*, 7, 197-210, 1974.
- Hoppe, G., V. Schytt, A. Haggblom, and H. Osterholm, The glacial history of Hopen, *Geogr. Ann.*, 51, 185-192, 1969.
- Hughes, T. J., The great Cenozoic ice sheet, *Paleogeogr. Palaeoclimatol. Palaeoecol.*, 50, 9-43, 1985.
- Hughes, T. J., Ice dynamics and deglaciation models when ice sheets collapsed, *North America and Adjacent Oceans During the Last Deglaciation*, vol K3, pp. 183-220, W. F. Ruddiman and H. E. Wright, Jr. eds., Geological Society of America, Boulder, 1987.
- Hughes, T. J., G. H. Denton, B. G. Andersen, D. H. Schilling, J. L. Fastook, and C. S. Lingle, The last great ice sheets: A global view, *The Last Great Ice Sheets*, 275-318, G. H. Denton and T. J. Hughes, eds., John Wiley and Sons, Inc., New York, 1981.

- Hughes, T. J., G. H. Denton, and J. L. Fastook, The Antarctica ice sheet: An analog for northern hemisphere paleo-ice sheets?, *Models in Geomorphology*, pp. 25-72, M. J. Woldenberg, ed., Allen and Unwin, Boston, 1985.
- Hyde, W. T., and W. R. Peltier, Sensitivity experiments with a model of the Ice Age cycle: The response to harmonic forcing, *J. Atmos. Sci.*, **42**, 2170-2188, 1985.
- Hyde, W. T., and W. R. Peltier, Sensitivity experiments with a model of the Ice Age cycle: the response to Milankovitch forcing, *J. Atmos. Sci.*, **44**, 1351-1374, 1987.
- Jones, G. A. and L. D. Keigwin, Evidence from Fram Strait (78°N) for early deglaciation, *Nature*, **336**, 56-59, 1988.
- Jones, G. A., and W. F. Ruddiman, Assessing the global meltwater spike, *Quat. Res.*, **17**, 148-172, 1982.
- Lea, P. D. and C. F. Waythomas, Late Pleistocene eolian sand sheets in central and southwestern Alaska, paper presented at Seventeenth Annual Arctic Workshop, INSTAAR, University of Colorado, Boulder, April 14-16, 1988.
- Markgraf, V., Paleoclimates of the Southern Argentine Andes, *Current Res. Pleistocene*, **4**, 150-157, 1987.
- McConnel, R. K., Viscosity of the mantle from relaxation time spectra of isostatic adjustment, *J. Geophys. Res.*, **73**, 7089-7105, 1968.
- Mercer, J. H., Antarctic ice and Sangamon sea level, *Int. Assoc. Sci. Hydrol. Publ.*, **79**, 217-225, 1968.
- Milankovitch, M., Canon of insolation and the ice-age problem, *K. Serb. Akad. Geogr. Spec. Publ.*, **132**, 484? pp., 1941.
- Milling, M. E., Geological appraisal of foundation conditions, northern North Sea, *Oceanol. Int.*, **75**, 310-318, 1975.
- Mitrovica, J. X. and W. R. Peltier, Pleistocene deglaciation and the global gravity field, *J. Geophys. Res.*, **94**, 13651-13671, 1990.
- Mix, A. C., The oxygen-isotope record of glaciation, *North America and Adjacent Oceans During the Last Deglaciation*, pp. 111-135, W.F. Ruddiman and H.E. Wright, Jr., eds., Geological Society of America, Boulder, 1987.
- Mix, A. C. and W. F. Ruddiman, Oxygen-isotope analysis and Pleistocene ice volumes, *Quat. Res.*, **21**, 1-20, 1984.
- North, G. R., R. F. Cahalan, and J. A. Coakley, Jr., Energy balance climate models, *Rev. Geophys.*, **19**, 91-121, 1981.
- Olausson, E., Evidence of climatic changes in North Atlantic deep-sea cores, with remarks on isotopic paleotemperature analysis, *Prog. Oceanog.*, **3**, 221-252, 1965.
- Olsson, I. U., and W. Blake, Jr., Problems of radiocarbon dating of raised beaches based on experience in Spitsbergen, *Norsk Geogr. Tidsskr.*, **18**, 47-64, 1962.
- Pearson, G. W., J. R. Pilcher, M. G. I. Baillie, D. M. Corbett, and F. Qua, High-precision ¹⁴C measurements of Irish oaks to show the natural ¹⁴C variations from AD 1840 to 5210 BC, *Radiocarbon*, **28(2B)**, 911-934, 1986.
- Peltier, W. R., The impulse response of a Maxwell Earth, *Rev. Geophys.*, **12**, 649-669, 1974.
- Peltier, W. R., Glacial isostatic adjustment, II The inverse problem, *Geophys. J.R. Astr. Soc.*, **46**, 669-706, 1976.
- Peltier, W. R., Dynamics of the ice age Earth, *Adv. in Geophys.*, **24**, 1-146, 1982.
- Peltier, W. R., New constraints on transient lower mantle rheology and internal mantle buoyancy from glacial rebound data, *Nature*, **318**, 614-617, 1985.
- Peltier, W. R., Lithospheric thickness, Antarctic deglaciation history, and ocean basin discretization effects in a global model of postglacial sea level change: A summary of some sources of non-uniqueness, *Quat. Res.*, **29**, 93-112, 1988a.
- Peltier, W. R., Global sea level and Earth rotation, *Science*, **240**, 895-901, 1988b.
- Peltier, W.R., Mantle viscosity, *Mantle Convection, Plate Tectonics and Global Dynamics*, pp. 389-478, Gordon Beach Science Publishers, New York, 1989.
- Peltier, W. R. and J. T. Andrews, Glacial isostatic adjustment, I The forward problem, *Geophys. J.R. Astr. Soc.*, **46**, 605-646, 1976.
- Peltier, W. R., W. E. Farrell, and J. A. Clark, Glacial isostasy and relative sea level: A global finite element model, *Tectonophysics*, **50**, 81-110, 1978.
- Peltier, W. R., R. A. Drummond, and A. M. Tushingham, Post-glacial rebound and transient lower mantle rheology, *Geophys. J.R. Astr. Soc.*, **87**, 79-116, 1986.
- Polanski, J., The maximum glaciation in the Argentine Cordillera, International Studies on the Quaternary, *Geol. Soc. Am. Spec. Pap.*, **84**, 453-472, 1965.
- Prest, V. K., The late Wisconsin glacier complex, *Geol. Surv. Can. Pap.*, **84-10**, map 1584A, 1984.
- Quinlan, G. M., Numerical models of post-glacial relative sea level changes in Atlantic Canada and the eastern Canadian Arctic., Ph.D. thesis, 499 pp., Dalhousie Univ., Halifax, Nova Scotia, 1981.
- Rodbell, D. T. and P. W. Birkeland, Glacial geology and glacial lacustrine sedimentology of Cordillera Central, northern Peruvian Andes, paper presented at Seventeenth Annual Arctic Workshop, INSTAAR, University of Colorado, Boulder, April 14-16, 1988.
- Schytt, V., G. Hoppe, W. Blake, Jr., and M. G. Grosswald, The extent of the Würm glaciation in the European Arctic, *IUGG Publ.*, **79**, pp. 207-216, Int. Assoc. Sci. Hydrol., General Assembly of Bern 1967, 1968.
- Shackleton, N. J. Oxygen isotope analysis and Pleistocene temperatures re-assessed, *Nature*, **215**, 15-17, 1967.
- Shackleton, N. J., and N. D. Opdyke, Oxygen isotope stratigraphy of equatorial Pacific core V28-238: Oxygen isotope temperatures and ice volumes on a 10⁵ year and 10⁶ year scale, *Quat. Res.*, **3**, 39-55, 1973.
- Shackleton, N. J., and N. D. Opdyke, Oxygen-isotope and paleomagnetic stratigraphy of Pacific core V28-239 late Pleistocene to latest Pleistocene, *Investigations in Late Quaternary Paleoceanography and Paleoclimatology*, pp. 449-464, R. M. Cline and J. D. Hays, eds., Geological Society of America, Memoir 145, 1976.
- Shackleton, N. J., and E. Vincent, Oxygen and carbon isotope studies in recent foraminifera from the southwest Indian Ocean, *Mar. Micropaleontol.*, **3**, 1-13, 1978.
- Shackleton, N. J., J. Imbrie, and M. A. Hall, Oxygen and carbon isotope record of East Pacific core V19-30, *Earth Planet. Sci. Lett.*, **65**, 233-244, 1983.
- Shilts, W. W., Flow patterns in the central North American ice sheet, *Nature*, **286**, 213-218, 1980.
- Shilts, W. W., Quaternary events - Hudson Bay Lowlands and southern district of Keewatin, *Geol. Surv. Can. Pap.*, **84-10**, 117-126, 1984.
- Shilts, W. W., Geological models for the configuration, history and style of disintegration of the Laurentide Ice Sheet, *Models in Geomorphology*, pp. 73-91, M. J. Woldenberg, ed., Allen and Unwin, Boston, 1985.
- Shilts, W. W., C.M. Cunningham, and C. A. Kaszycki, Keewatin Ice Sheet - Re-evaluation of the traditional concept of the Laurentide ice sheet, *Geology*, **7**, 537-541, 1979.
- Stuiver, M., G. H. Denton, T. J. Hughes, and J. L. Fastook, History of marine ice sheets in West Antarctica, *The Last Great Ice Sheets*, pp. 319-436, G.H. Denton and T. J. Hughes eds., John Wiley and Sons, Inc., New York, 1981.
- Stuiver, M., G. W. Pearson, and T. F. Braziunas, Radiocarbon age calibration of marine samples back to 9000 cal. yr. bp., *Radiocarbon*, **28(2B)**, 980-1021, 1986.
- Sundvor, E., Seismic refraction and reflection measurements in the Southern Barents Sea, *Mar. Geol.*, **16**, 255-273, 1974.
- Tyrrell, J. B., The glaciation of north central Canada, *J. Geol.*, **6**, 147-160, 1898.
- Urey, H. C., The thermodynamic properties of isotopic substances, *J. Chem. Soc.*, 562-581, 1974.
- Veeh, H. H. and J. Chappell, Astronomical theory of climate: Support from New Guinea, *Science*, **167**, 862-865, 1970.
- Vergnaud-Grazzini, C., Non-equilibrium isotopic compositions of shells of planktonic foraminifera in the Mediterranean Sea, *Palaeogeogr. Palaeoclimatol. Palaeoecol.*, **320**, 263-276, 1976.
- Vincent, J.-S., La géologie du Quaternaire et la géomorphologie de l'île Banks, Arctic Canadian, *Geol. Surv. Can. Mem.*, **405**, 118?(please give inclusive pages of article) p., 1983.

- Vincent, J.-S., Quaternary stratigraphy of the western Canadian Arctic Archipelago, *Geol. Surv. Can. Pap.*, 84-10, 87-100, 1984.
- Volkov, I. A., M. G. Grosswald, and S. L. Troitsky, On the proglacial drainage during the last glaciation of West Siberia, *Izv. Akad., Nauk SSSR Ser. Geogr.* 4, 25-35, 1978.
- Wu, P., and W. R. Peltier, Glacial isostatic adjustment and free air gravity

anomaly as a constraint on deep mantle viscosity, *Geophys. J. R. Astron. Soc.*, 74, 377-450 1983.

(Received February 2, 1990;
revised July 13, 1990;
accepted July 18, 1990)